AMERICAN INSTITUTE OF AERONAUTICS AND ASTRONAUTICS

1290 AVENUE OF THE AMERICAS
NEW YORK, N.Y. 10019
TELEPHONE
212/581-4300

March 15, 1979

TO: Mrs. Winnie M. Morgan

FROM: Ruth F. Bryans, Administrator, Scientific Publications

A back-up paper is enclosed for the following Synoptic:

Author(s): J. F. Foss

Title of Synoptic: "Measurements in a Large Angle Oblique Jet Impingement Flow" - Log No. J10975

Title of Back-up Paper: Same as above

Correspondence with: Professor J. F. Foss
Falkenweg 27
D7500 Karlsruhe - Dammerstock
Karlsruhe, WEST GERMANY

Journal: AIAA Journal

Scheduled Issue: July 1979

Ruth F. Bryans

(Miss) Ruth F. Bryans

Enclosure

MEASUREMENTS IN A LARGE ANGLE OBLIQUE JET IMPINGEMENT FLOW

By

John F. Foss

August 7, 1978

Backup Document for AIAA Synoptic Scheduled for
Publication in the AIAA Journal, July 1979

Department of Mechanical Engineering
Michigan State University
East Lansing, Michigan

SYNOPTIC BACKUP DOCUMENT

This document is made publicly available through the NASA scientific and technical information system as a service to readers of the corresponding "Synoptic" which is scheduled for publication in the following (checked) technical journal of the American Institute of Aeronautics and Astronautics.

- [X] AIAA Journal, July 1979
- [ ] Journal of Aircraft
- [ ] Journal of Spacecraft & Rockets
- [ ] Journal of Hydronautics

A Synoptic is a brief journal article that presents the key results of an investigation in text, tabular, and graphical form. It is neither a long abstract nor a condensation of a full length paper, but is written by the authors with the specific purpose of presenting essential information in an easily assimilated manner. It is editorially and technically reviewed for publication just as is any manuscript submission. The author must, however, also submit a full backup paper to aid the editors and reviewers in their evaluation of the synoptic. The backup paper, which may be an original manuscript or a research report, is not required to conform to AIAA manuscript rules.

For the benefit of readers of the Synoptic who may wish to refer to this backup document, it is made available in this microfiche (or facsimile) form without editorial or makeup changes.

Measurements In A Large Angle Oblique Jet Impingement Flow*

John F. Foss
Department of Mechanical Engineering
Michigan State University
East Lansing, Michigan

Member AIAA

*Work Supported by NASA Langley Research Center under NGR 23-004-091

INTRODUCTION

The flow field associated with the oblique impingement of an axisymmetric jet is of interest as a result of its presence in numerous technological problems. Prominent among these is the externally blown flap (e.b.f.) configuration for STOL aircraft. The e.b.f. configuration and the oblique jet impingement flow, as its laboratory counterpart, are shown schematically in Figures 1 and 2.

A comprehensive investigation of the shallow angle ($0 \leq \alpha \lesssim 15°$) oblique impingement flow is summarized by Foss and Kleis [1976]. The passive and active spreading characteristics of this flow, the role of the initially azimuthal vorticity field and an analysis of the stagnation point region are presented in this Synoptic; the substantial data base from which these results are inferred is available in the reference manuscript and reports to the NASA which were summarized in this publication.

The large angle oblique jet impingement flow field is rather more complex than its shallow angle counterpart. The dominant streamwise motion of the latter is replaced by a fully 360° flow field albeit the streamwise character of the initial jet is manifest in the velocity field of the spreading jet. Prior experimental studies provide some insight into the structure of the large angle flow field. Donaldson and Snedecker [1971] investigated a wide range of Mach numbers, jet-plate spacings, angles, and impact plate dimensions via surface pressure and centerplane velocity measurements. Westley et.al. [1972] provide surface r.m.s. pressure measurements. Fink [1973] has examined the acoustic characteristics of the large-angle impinging jet flows and has advanced some interpretations of the probable turbulence structure associated with them. Other investigations which focused exclusively on the acoustic characteristics of this flow include Olsen, et. al. [1972], Putnam and Lasagna [1972], Hass [1972] and Yu et. al. [1974].

Given the information base of these studies, and recognizing the motivation of the e.b.f. configuration, a detailed study of the $\alpha = 45°$, $L/d = 7$ oblique jet impingement flow was deemed to be appropriate. The Reynolds number, $u_o d/\nu$, was 4.8×10^4, this value is considered to be sufficiently large that qualitatively similar results are expected for larger

Reynolds numbers which may be found in flows of technological interest.

EXPERIMENTAL FACILITY

The requirement to execute spatial (e.g. vertical or radial) traverses, with a probe alignment which could be used to infer the flow direction in planes parallel to that of the impact plate, was achieved with the flow and traverse systems shown in Figures 3 and 4. Pressurized air from a large plenum chamber was supplied through a flexible conduit and into the tube shown in Figure 3. The support structure allowed the tube to be rotated around the jet axis-impact plate intersection point. The traverse of the probe was executed along a line perpendicular to the lathe bed and at continuously variable locations above the impact plate. The probe could be pivoted about its measurement point to align the probe with the local mean velocity. The probe positioning and data acquisition were executed under the software control of a minicomputer. Standard hot-wire equipment (Disa gold-plated probe, T.S.I. 1054A anemometer) and pressure transducer (Decker Corp.308-3) were used.

DATA ACQUISITION SYSTEM AND MEASUREMENT TECHNIQUES

A Texas Instruments 960 A minicomputer is the central component in the data acquisition system (see Figure 4). This unit is used to position the probe at the r, z values prescribed for the traverse (e.g., 13 data points at $z = 0.05\ d$, $0 \leq r \leq 4$ in.) by means of analog voltage signals used to drive the stepping motors, to record the data for a prescribed time period (e.g., 60 second averaging time), and to orient the probe into the mean flow direction of the r,Θ plane by a scheme which relies upon the symmetric and approximately cosine response of a yawed hot-wire probe. The probe is positioned at ± 45, ± 30, ± 15, and 0 degrees with respect to the presumed flow direction (the direction found in the previous reading of the traverse), and the time-mean flow direction (β_o) is calculated by the following technique. The mean hot-wire response at each of the seven positions $\overline{E}_i$ (β_i), is divided by the maximum voltage, $\overline{E}_{max}$, recorded during the seven readings, and the apparent angle of the probe with respect to the head-on condition ($\beta_i - \beta_{oi}$) is calculated from the relationship

$$\frac{E_1}{E_{max}} = \cos(\beta_i - \beta_{oi}). \quad (1)$$

The time-mean flow angle, $\bar{\beta}_o$, is then calculated from the relationship

$$\bar{\beta}_o = \frac{1}{7} \sum_{i=1}^{7} \beta_{oi}. \quad (2)$$

The voltage values from the hot-wire probe are digitized and initially processed in the minicomputer such that subsequent processing will result in the mean velocity and turbulence quantities expressed in laboratory coordinates, viz., $\bar{u}_r$, $\bar{u}_\theta$, $\overline{u_r^2}$, $\overline{u_\theta^2}$, $\overline{u_r u_\theta}$. Specifically, let e_0, e_1, and e_2 be voltage values from the hot-wire probe as it is oriented at β_o and at $\beta_o \pm 45$ degrees respectively. The desired functions of the velocity are obtained from these voltage values following their digitally computed averages. Let $[f(e_k^a)]_j$ represent one sample, j, of a function, f, of the voltage, e_k; viz., $f(e_k^a)$: e_0, e_1, e_2, e_0^2, e_1^2, e_2^2. The average value of $f(e_k^a)$ is computed as

$$\langle f(e_k^a) \rangle = \frac{1}{N} \sum_{j=1}^{N} [f(e_k^a)]_j \quad (3)$$

A typical N value is 6×10^5 which represents a 30 second sample at a sampling rate of 20 Khz. The magnitude of the velocity, $[\bar{u}_r^2 + \bar{u}_\theta^2]^{1/2}$, is obtained from $\langle f(e_0) \rangle$ and $\bar{u}_r$, $\bar{u}_\theta$ follow from the known β_o value. The intensity of the streamwise fluctuations is determined from $\{\langle f(e_0^2) \rangle - [\langle f(e_0) \rangle]^2\}^{1/2}$. The intensity of the lateral fluctuations and the correlation between the two fluctuating components follows from the assumed cosine law response and the numerical quantities $0.25\{\langle f(e_2^2) \rangle - \langle f(e_3^2) \rangle\}$ and $\langle f(e_2^2) \rangle - \langle f(e_0^2) \rangle - 0.125\{\langle f(e_2^2) \rangle - \langle f(e_3^2) \rangle\}$. See, for example, Hinze [1959, 1975] for the derivation. The $\langle f(e_k^a) \rangle$ values are recorded for specified traverses; the average values are then transferred to the IBM 1800 computer where the voltages are converted to velocities via the response equations of the wires and the fourth order polynomial used to fit the calibration, $e = e(u)$, of the "linearized" hot-wire probes. Two mean velocity and three Reynolds stress terms are known at the given

point in terms of probe coordinates (s,t,z). The data can then be transformed to (r,θ, z) coordinates. The approximate nature of the "cosine-law" angular response equation limits the accuracy of the $\overline{u_\theta^2}$ and $\overline{u_r u_\theta}$ values. See, for example, Friehe and Schwarz [1968] for a more accurate representation of the yaw effect.

RESULTS

The data representing the time mean surface pressure field measurements have been collectively presented in the form of surface isobars; these are shown on Figure 5. An expanded scale to better delineate the maximum pressure region is used in Figure 6.

The velocity field information was collected in three separate data acquisition runs. Traverses in the $\theta = 0, \pi$ plane were made in the jet prior to its impact on the plate and also downstream of the geometric impact point. These data are shown in Figure 7. These results indicated that a local maxima in the velocity occurred near $z/d = 0.053$ ($z = 0.04$ in.). Hence, this elevation was selected as the location of the plane for the radial traverses to define the velocity field near the plate. A composite view of this velocity field is presented in Figure 8. The vertical velocity traverses to complete the exploratory documentation were taken at $r/d = 1$ and $r/d = 3$ and at the angles $\theta = \pi/4$ and $\pi/2$. These results are presented in Figure 9. In addition to the graphical presentation, a listing of the data is provided in Appendix A. As discussed below, there is reason to suspect the detailed values from the $\pi/3$ and $\pi/6$ radial traverses. Hence, these have been excluded from the listing even though they are considered to be sufficiently accurate to be included in the composite plot of Figure 8.

In order to complete the graphical documentation of the radial velocity traverses, it was decided to adopt a presentation format which would allow the relative importance of the various turbulence kinetic energy production terms to be assessed. These data are shown in Figures 10 to 13. Since the radial traverses were taken in even increments ($\Delta r/d = 2/3$) it is possible to construct both radial and azimuthal plots of the radial and azimuthal mean velocities, fluctuating velocity intensities and fluctuating velocity correlations (kinematic Reynolds stress).

In order to facilitate the comparison of the production effects, the vertical ordinates were essentially maintained at constant values for all plots. The abscissa scale for the radial traverse presentations was kept constant for all plots. The abscissa length is contracted approximately 50 percent for the azimuthal plots, hence, the gradients appear to be too large by this factor. An additional radial traverse which makes use of a somewhat finer series of probe locations and which is slightly closer to the plate is presented in Figure 14.

The azimuthal plots of the radial traverse data revealed apparant inconsistancies from the $\Theta = \pi/3$ and $\pi/6$ runs. Consequently, these data were removed from Figures 10 to 13 and the data listings of Appendix A.

DISCUSSION OF RESULTS

There are two principal characteristics of the large angle impingement flow which have been deduced from the data base represented by the results discussed above. The first characteristic is that the flow field near the plate demonstrates two distinct "symmetry"* patterns, one is "centered" near the location of the maximum surface pressure and the second is a symmetry pattern about the geometric intersection of the jet axis with the plate and is realized when the flow reaches a sufficiently large radial distance. The second characteristic is that the turbulence kinetic energy in the region above the plate is not significantly greater than that which can be accounted for by the convection of turbulence energy by the mean motion. The data which allow the inference of these two characteristics and an evaluation of the pressure field in the neighborhood of the stagnation point are presented in the following subsections.

Symmetry Characteristics of the Flow near the Surface

An overall picture of the flow pattern near the surface of the plate is provided by combining the data from all of the radial traverses in such a manner that the magnitude and direction of the velocity in the $z/d = 0.053$ plane is revealed. This plot is presented in Figure 8.

*The word "symmetry" is not meant to imply azimuthal independence of the velocity fields; e.g., at a given r, $\bar{u}_r(0) > \bar{u}_r(\pi)$. The "symmetry point" is rather like a non-axisymmetric source location.

The symmetry "point" for the neighborhood of the maximum pressure is approximately $\theta = \pi, r/d = 0.87$ (see Figure 7) and a "local symmetry" of the $\underset{\sim}{V}(r,\theta)$ field about this location is suggested by the data of the composite plot. Considerably more data in this region and a more sophisticated measurement technique, which is capable of segregating the r, θ, and z velocity components, would be required to improve the quantitative assessment of this flow pattern.

For sufficiently large r values ($r/d \approx 3$ which represents an r/z value of approximately 55) the flow pattern near the surface evolves such that the geometric intersection of the jet axis and the plate is the symmetry "point". The radial traverse data for $\bar{v}_\theta/u_o$ (see Figure 11) demonstrates this effect quantitatively and the vanishing $\overline{u_r v_\theta}$ values (see Figure 12) from the same traverses similarly confirm this observation. The azimuthal variation of $\bar{u}_r/u_o$ (see Figure 12) shows that the flow is not axisymmetric about the symmetry point (this is an expected result since the jet inclination is $\pi/4$, not $\pi/2$ radians with respect to the plate) but these distributions also show that the variation with respect to θ becomes rather slight as r increases. It is important to recall that these results are for the region quite close to the plate. The flow at a sufficient elevation above the plate will retain its predominant $\theta \approx 0$ orientation. The surface velocity pattern is corroborated by the visualization studies of Westley, et. al. [1972].

The governing mechanics which result in these symmetry patterns are not fully revealed by these data. Without direct measurements of $\bar{w}(r,\theta)$ and $\overline{u_r w_z}$ and considerably more comprehensive data, such an assessment would not be feasible. However, the local symmetry about the maximum pressure strongly suggests that the pressure gradient is the dominant term in the equation of motion for this region of the flow.

The effects which lead to symmetry about the geometric origin are much more obscure. The surface static pressure field is clearly not symmetric about the origin and this would suggest that the local effects leading to such symmetry are the Reynolds stresses, i.e., $\overline{u_r v_\theta}$ and $\overline{v_\theta^2}$. It seems clear that the global symmetry of the entire jet is involved in the processes which lead to this result. However it is not a simple matter to connect the global effects to the Reynolds stresses which must be responsible for the local accelerations required to give the observed

symmetry. One mechanistic feature which has the potential for such an effect is the predominant azimuthal vorticity of the approaching jet.

The Turbulence Field near the Plate Surface

The presence of the plate with the consequent no slip condition and the strong velocity gradients might lead to the apriori expectation that the turbulence energy level near the plate is greater than that to be expected if the plate were absent. This expectation is not supported by the data.

Figure 15 has been prepared as a composite plot of the turbulence intensity information from the radial traverses. In order to compare the turbulence levels near the plate with the turbulence level of the jet itself, the data for the condition $z/d = 0.053$ and $\theta = 90$ degrees has been plotted on the same figure with the radial traverse data of $x/d = 6$ and 8, from Kleis and Foss [1974], see Figure 16. This comparison appears to be the most reasonable basis from which to evaluate the relative turbulence level created by the impingement process given the available experimental data. However, it is not unambiguous. A preferrable comparison would be on the basis of a volume integral of the turbulence energy in a given streamwise domain. Such an integral could be readily formulated for the axisymmetric case but would require an extensive series of traverses in the three-dimensional impingement flow. The vertical traverse data of Figure 9 show that the turbulence intensity magnitudes in the plane $z/d = 0.053$ are representative of the maximum values for these quantities in the impingement flow albeit there is a slight increase in the steep gradient $(\partial \bar{u}_{\_}/\partial z)$ region for $z < 0.053d$.

The suppression of the turbulence intensity and the Reynolds stresses by concave curvature is discussed, along with numerous other effects, at length by Bradshaw [1973]. The present observations regarding the maximum turbulence intensity values are compatible with these considerations. The r.m.s. surface pressure data of Westley, et.al. [1972] indicate two maxima located up and downstream of the origin. Apparently, these are related to the stagnation point and to the local maxima in the turbulence intensity magnitudes observed in the present data.

Stagnation Point

A technique of identifying the stagnation streamline by comparing the measured velocity near the plate's surface with the surface static pressure taps was successfully employed by Foss and Kleis [1976] to demonstrate that the stagnation point is considerably upstream of the maximum pressure location and near the zero surface isobar for the shallow angle impingement flow field. A necessary characteristic of this technique is that the static pressure at the location of the velocity measurement be equal to the atmospheric value. In the earlier study, an over-pressure at the velocity measuring location would have resulted in a farther upstream movement of the inferred stagnation point.

The same technique cannot be applied to the measurement of the stagnation point in the large angle case. This result is based upon the following observations: (i) the local symmetry of the velocity field (see Figure 8) requires that the stagnation point be in the neighborhood of $x/d \simeq -1$ and (ii) the static pressure at the location of the velocity measurement must be greater than zero. The latter observation is based upon a comparison of the measured surface static pressures and the inferred dynamic pressure at the stagnation point. Specifically, from Figure 6,

$$p \ (r/d = 1, \ \theta = \pi) = \rho \bar{u}_o^2 \ (0.2) + p_{atm} \cong p_{stag} \qquad (4)$$

and from Figure 7, the velocity magnitude in this neighborhood of the approaching jet is of the order of $0.3\, u_o$. The stagnation pressure for such a condition is given by

$$p_{stag} = p + \rho \ u_o^2 \ (0.045) \qquad (5)$$

Comparing the two equations, it is apparant that the static pressure at the measuring point must be of the order of $0.16\ \rho\ u_o^2$.

Conclusions

The following conclusions are supported by the results of this study.

1) The plane defined by $z/d \simeq 0.05$ is in the neighborhood of the maximum velocity over most of the plate. Hence, this is also a plane separating regions of opposite sense mean vorticity. (Note that $\partial \bar{u}_s / \partial z >> \partial \bar{w} / \partial s$).

2) The flow in the z/d≈0.05 plane (and presumably for smaller z/d values) can be characterized in terms of two symmetry patterns. Specifically, a local symmetry about the inferred stagnation point (x/d -0.8) for the near region and symmetry about the intersection of the jet axis and the plate (r/d = 0) for larger radius values. The latter effects are predominant for r/d $\gtrsim$ 3.

3) The maximum levels of the turbulent fluctuations in the region near the plate are not larger than the turbulence levels of the approach jet. Insufficient data is available to establish whether or not the jet / plate interaction results in an increase in the total turbulence kinetic energy.

4) Quantitative estimates of the terms in the equations of motion indicate that significant pressure magnitudes may be expected within the jet in the neighborhood of the stagnation point.

References

Bradshaw, P., "Effects of streamline curvature on turbulent flow." AGARD o graph No. 169, August 1973.

Donaldson, C. DuP. and R. Snedecker, "A Study of free jet impingement, Part 1. Mean properties of free and impinging jets," Journal Fluid Mechanics, Vo. 45, p. 2, 1971.

Fink, M.R., "Mechanisms of externally blown flap noise," AIAA Paper No. 73-1029, Oct. 1973.

Foss, J.F., "The VORCOM, part 1 Analytical Considerations," NASA Report, Grant NGR 23-004-091, June 1976.

Foss, J.F. and Kleis, S.J. "Mean Flow characteristics for the Oblique impingement of an axisymmetric jet." AIAA Jour., Vol. 14, No. 6, p. 705, June 1976.

Friehe, C.A. and Schwarz, W.H. "Deviations from the cosine law for yawed cylindrical hot-wire sensors." Jour. Applied Mech., Trans ASME Vol. 35, pp 655-662, (1968).

Haas, M., "Blown flap noise," MIT Report FTL 72-5, 1972.

Hinze, J.O. Turbulence, McGraw Hill Book Co. New York, First Ed. 1959, Second Ed. 1975.

Kleis, S.J. and J.F. Foss, "The effects of exit conditions on the development of an axisymmetric turbulent free jet," Third Year Technical Report, Grant No. NGR 23-004-068, (1974).

Olsen, W., J. Miles, and R. Dorsch, "Noise generated by impingement of a jet upon a large flat board," TN D-7075, 1972, NASA, Cleveland, Ohio.

Putnam, T.W. and P.L. Lasagna, "Externally blown flap impingement noise," AIAA Paper No. 72-664, 1972.

Westley, R., J.H. Woolley, and P. Brosseau, "Surface pressure fluctuations from jet impingement on an inclined flat plate," AGARD Symposium on Acoustic Fatigue. 1972.

Yu, J.C., Reddy, N.N., and Whitesides, J.L. Jr. "Noise and Flow Characteristics of an externally blown flap." Second Interagency Symposium on Univ. Research in Transportation Noise Ed. by G. Banerian and W.F. Reiter North Carolina State U. and Dept. of Transportation - June, 1974.

Appendix: Tabular Listing of the Experimental Data

RADIAL TRAVERSE JET AT 0 DEGREES

r/d	z/d	β	$\|\bar{V}\|/u_o$	$\bar{u}_r/u_o$	$\bar{v}_\theta/u_o$	$\bar{u}_r^2/u_o^2$	$\bar{v}_\theta^2/u_o^2$	$\overline{u_r v_\theta}/u_o^2$
8.000	0.053	0.3	26.5	26.5	0.1	^.93	0.24	0.00
7.333	0.053	0.0	29.5	29.5	0.0	1.11	0.28	0.00
6.666	0.053	0.1	32.8	32.8	0.0	1.29	0.36	0.00
6.000	0.053	0.1	37.2	37.2	0.0	1.47	0.46	-0.00
5.333	0.053	-0.3	41.7	41.7	-0.2	1.65	0.55	0.01
4.666	0.053	-0.0	47.8	47.8	-0.0	1.73	0.67	0.00
4.000	0.053	-0.0	54.6	54.6	-0.0	1.73	0.67	-0.00
3.333	0.053	0.2	61.2	61.2	0.2	1.68	0.64	-0.00
2.666	0.053	-0.0	67.8	67.8	-0.0	1.73	0.45	-0.00
2.000	0.053	-0.1	73.3	73.3	-0.1	1.83	0.36	-0.00
1.333	0.053	-0.3	75.9	75.9	-0.5	2.06	0.40	-0.01
0.666	0.053	-0.6	71.6	71.6	-0.8	2.36	0.76	0.00
0.000	0.053	-1.3	51.7	51.7	-1.2	2.71	1.30	-0.00

Note: β is in degrees; columns 4 - 9 are expressed as percentages

RADIAL TRAVERSE JET AT 15 DEGREES

r/d	z/d	β	$\lvert\overline{V}\rvert/u_o$	$\overline{u}_r/u_o$	$\overline{v}_\theta/u_o$	$\overline{u_r^2}/u_o^2$	$\overline{v_\theta^2}/u_o^2$	$\overline{u_r v_\theta}/u_o^2$
8.000	0.053	-0.1	26.2	26.2	-0.0	0.92	0.26	-0.01
7.333	0.053	-0.3	29.0	29.0	-0.1	1.10	0.27	-0.01
6.666	0.053	-0.0	32.3	32.3	-0.0	1.29	0.37	-0.02
6.000	0.053	1.0	36.6	36.6	0.6	1.49	0.46	-0.03
5.333	0.053	1.3	41.4	41.4	0.9	1.66	0.58	-0.04
4.666	0.053	1.7	46.9	46.9	1.4	1.78	0.65	-0.05
4.000	0.053	2.2	53.9	53.6	2.1	1.80	0.72	-0.04
3.333	0.053	2.7	60.8	60.8	2.9	1.81	0.61	-0.02
2.666	0.053	3.1	67.7	67.6	3.7	1.83	0.48	0.01
2.000	0.053	4.1	73.5	73.3	5.3	1.95	0.38	0.07
1.333	0.053	5.4	76.8	76.4	7.3	2.19	0.45	0.16
0.666	0.053	8.6	73.3	71.4	10.8	2.46	0.88	0.28
0.000	0.053	16.1	52.4	50.3	14.5	2.65	1.53	0.39

Note: β is in degrees; columns 4 - 9 are expressed as percentages

RADIAL TRAVERSE JET AT 45 DEGREES

r/d	z/d	β	$\|V\|/u_o$	$\bar{u}_r/u_o$	$\bar{v}_\theta/u_o$	$\overline{u_r^2}/u_o^2$	$\overline{v_\theta^2}/u_o^2$	$\overline{u_r v_\theta}/u_o^2$
8.000	0.053	0.6	16.8	16.8	0.1	0.37	0.14	-0.01
7.333	0.053	1.0	18.6	18.6	0.3	0.47	0.15	-0.01
6.666	0.053	1.3	20.5	20.5	0.4	0.57	0.19	-0.01
6.000	0.053	2.5	23.3	23.3	1.0	0.73	0.23	-0.01
5.333	0.053	3.5	26.8	26.7	1.6	0.94	0.28	-0.01
4.666	0.053	4.7	31.2	31.1	2.5	1.19	0.34	-0.00
4.000	0.053	6.5	37.0	36.8	4.2	1.43	0.44	0.00
3.333	0.053	8.5	44.5	44.0	6.6	1.57	0.54	0.00
2.666	0.053	10.5	52.6	51.7	9.6	1.65	0.54	0.06
2.000	0.053	13.0	60.8	59.2	13.7	1.79	0.55	0.18
1.333	0.053	17.1	67.0	64.0	19.8	2.09	0.68	0.43
0.666	0.053	25.9	65.5	58.9	28.6	2.17	1.26	0.71
0.000	0.053	48.6	50.6	33.4	38.0	1.83	2.14	0.66

Note: β is in degrees; columns 4 - 9 are expressed as percentages

RADIAL TRAVERSE JET AT 90 DEGREES

r/d	z/d	β	$\lvert\bar{V}\rvert/u_o$	$\bar{u}_r/u_o$	$\bar{v}_\theta/u_o$	$\bar{u}_r^2/u_o^2$	$\bar{v}_\theta^2/u_o^2$	$\overline{u_r v_\theta}/u_o^2$
8.000	0.053	5.2	8.5	8.4	0.7	0.08	0.01	0.00
7.333	0.053	5.3	9.4	9.3	0.8	0.10	0.03	0.00
6.667	0.053	6.8	10.7	10.6	1.2	0.14	0.04	0.00
6.000	0.053	6.7	12.3	12.2	1.4	0.18	0.06	0.00
5.334	0.053	7.7	14.4	14.2	1.9	0.25	0.09	0.01
4.667	0.053	10.2	16.8	16.6	2.9	0.36	0.12	0.02
4.001	0.053	11.1	20.5	20.2	3.9	0.54	0.17	0.05
3.334	0.053	15.4	26.5	25.6	7.0	0.81	0.24	0.13
2.667	0.053	21.2	34.8	32.5	12.6	1.09	0.41	0.25
2.001	0.053	28.3	45.1	39.7	21.4	1.27	0.67	0.35
1.334	0.053	37.1	54.0	43.0	32.5	1.47	1.15	0.57
0.667	0.053	55.0	56.3	32.3	46.2	1.32	2.03	0.62

Note: β is in degrees; columns 4 - 9 are expressed as percentages

VERTICAL TRAVERSE JET AT 0 DEGREES

r/d	z/d	β	$\|\overline{V}\|/u_o$	$\overline{u}_r/u_o$	$\overline{v}_\theta/u_o$	$\overline{u}_r^2/u_o^2$	$\overline{v}_\theta^2/u_o^2$	$\overline{u_r v_\theta}/u_o^2$
3.000	0.053	0.0	58.2	58.2	-	1.53	-	-
3.000	0.066	0.0	66.0	66.0	-	1.45	-	-
3.000	0.080	0.0	62.0	62.0	-	1.37	-	-
3.000	0.093	0.0	62.2	62.2	-	1.29	-	-
3.000	0.106	0.0	61.9	61.9	-	1.24	-	-
3.000	0.120	0.0	61.3	61.3	-	1.17	-	-
3.000	0.133	0.0	60.2	60.2	-	1.13	-	-
3.000	0.146	0.0	59.0	59.0	-	1.12	-	-
3.000	0.160	0.0	57.6	57.6	-	1.13	-	-
3.000	0.173	0.0	55.9	55.9	-	1.12	-	-
3.000	0.213	0.0	51.3	51.3	-	1.21	-	-
3.000	0.266	0.0	44.7	44.7	-	1.27	-	-
3.000	0.319	0.0	38.5	38.5	-	1.30	-	-
3.000	0.373	0.0	32.7	32.7	-	1.24	-	-
3.000	0.426	0.0	27.4	27.4	-	1.15	-	-
3.000	0.480	0.0	23.0	23.0	-	1.04	-	-
3.000	0.533	0.0	19.2	19.2	-	0.87	-	-
3.000	0.586	0.0	15.9	15.9	-	0.74	-	-
3.000	0.640	0.0	13.4	13.4	-	0.59	-	-
3.000	0.693	0.0	11.0	11.0	-	0.43	-	-
3.000	0.746	0.0	9.1	9.1	-	0.31	-	-
3.000	0.800	0.0	7.8	7.8	-	0.23	-	-
3.000	0.853	0.0	6.9	6.9	-	0.17	-	-
3.000	0.906	0.0	6.1	6.1	-	0.11	-	-
3.000	0.960	0.0	5.5	5.5	-	0.08	-	-
3.000	1.013	0.0	5.0	5.0	-	0.05	-	-
3.000	1.066	0.0	4.8	4.8	-	0.04	-	-

Note: β is in degrees; columns 4 - 9 are expressed as percentages

RADIAL TRAVERSE JET AT 135 DEGREES

r/d	z/d	β	$\|\overline{V}\|/u_o$	$\overline{u}_r/u_o$	$\overline{v}_\theta/u_o$	$\overline{u}_r^2/u_o^2$	$\overline{v}_\theta^2/u_o^2$	$\overline{u_r v_\theta}/u_o^2$
7.999	0.053	1.7	3.9	3.9	0.1	0.00	-0.00	0.00
7.333	0.053	3.9	4.3	4.3	0.2	0.01	-0.00	0.00
6.666	0.053	4.2	5.3	5.3	0.3	0.02	-0.00	0.00
5.999	0.053	5.5	6.3	6.3	0.6	0.04	0.00	0.00
5.333	0.053	8.3	7.7	7.6	1.1	0.07	0.01	0.00
4.666	0.053	8.6	9.6	9.5	1.4	0.12	0.03	0.01
3.999	0.053	12.0	12.5	12.3	2.6	0.22	0.06	0.02
3.333	0.053	16.3	16.8	16.1	4.7	0.38	0.13	0.07
2.666	0.053	26.6	24.2	21.7	10.8	0.66	0.31	0.23
1.999	0.053	37.5	35.1	27.8	21.4	0.98	0.86	0.40
1.333	0.053	54.4	41.4	24.0	33.6	1.12	1.85	0.53
0.666	0.053	82.4	42.3	5.5	42.0	0.17	2.42	0.29

Note: β is in degrees; columns 4 - 9 are expressed as percentages

RADIAL TRAVERSE JET AT 180 DEGREES

r/d	z/d	β	$\|\overline{V}\|/u_o$	$\overline{u}_r/u_o$	$\overline{v}_\theta/u_o$	$\overline{u_r^2}/u_o^2$	$\overline{v_\theta^2}/u_o^2$	$\overline{u_r v_\theta}/u_o^2$
8.000	0.053	-0.8	3.2	3.2	-0.0	-0.00	-0.01	-0.00
7.333	0.053	-3.8	3.7	3.7	-0.2	0.00	-0.01	0.00
6.666	0.053	0.4	4.0	4.0	0.0	0.01	-0.00	-0.00
6.000	0.053	0.7	4.6	4.6	0.0	0.02	-0.00	-0.00
5.333	0.053	-0.8	5.8	5.8	-0.0	0.04	-0.00	-0.00
4.666	0.053	-0.3	7.5	7.5	-0.0	0.08	0.00	-0.00
4.000	0.053	1.1	9.8	9.8	0.1	0.15	0.03	-0.00
3.333	0.053	0.2	13.7	13.7	0.0	0.30	0.08	0.00
2.666	0.053	1.5	20.2	20.2	0.5	0.68	0.24	0.01
2.000	0.053	3.3	24.4	24.3	1.4	1.19	0.56	0.04
1.333	0.053	7.3	17.9	17.8	2.3	0.73	0.71	0.04
0.666	0.053	-2.6	27.4	27.4	-1.2	1.92	0.81	-0.11

Note: β is in degrees; columns 4 - 9 are expressed as percentages

RADIAL TRAVERSE JET AT 30 DEGREES

r/d	z/d	β	$\lvert\bar{V}\rvert/u_o$	$\bar{u}_r/u_o$	$\bar{v}_\theta/u_o$	$\overline{u_r^2}/u_o^2$	$\overline{v_\theta^2}/u_o^2$	$\overline{u_r v_\theta}/u_o^2$
8.000	0.053	-0.5	20.2	20.2	-0.2	0.28	-0.07	-0.00
7.333	0.053	-0.7	21.9	21.9	-0.2	0.40	-0.09	-0.00
6.666	0.053	-0.6	24.0	24.0	-0.2	0.54	-0.10	-0.00
6.000	0.053	0.9	27.5	27.5	0.4	0.76	-0.10	0.00
5.333	0.053	1.5	31.0	31.0	0.8	0.96	-0.03	0.01
4.666	0.053	3.3	35.6	35.6	2.0	1.14	0.09	0.01
4.000	0.053	4.2	41.2	41.1	3.0	1.25	0.30	-0.00
3.333	0.053	5.3	47.8	47.6	4.4	1.24	0.44	0.00
2.666	0.053	6.8	54.1	53.7	6.4	1.20	0.46	0.01
2.000	0.053	8.5	59.9	59.2	8.9	1.22	0.44	0.07
1.333	0.053	11.4	63.8	62.5	12.6	1.34	0.49	0.17
0.666	0.053	17.4	61.6	58.8	18.4	1.49	0.78	0.30
0.000	0.053	32.2	47.2	39.9	25.1	1.55	1.13	0.54

Note: β is in degrees; columns 4 - 9 are expressed as percentages

RADIAL TRAVERSE JET AT 60 DEGREES

r/d	z/d	β	$\|\overline{V}\|/u_o$	$\overline{u}_r/u_o$	$\overline{v}_\theta/u_o$	$\overline{u_r^2}/u_o^2$	$\overline{v_\theta^2}/u_o^2$	$\overline{u_r v_\theta}/u_o^2$
8.000	0.053	2.3	20.9	20.9	0.8	0.19	0.36	-0.02
7.333	0.053	3.7	21.4	21.4	1.3	0.17	0.35	-0.01
6.666	0.053	3.7	22.1	22.0	1.4	0.18	0.31	-0.01
6.000	0.053	5.5	23.3	23.2	2.2	0.20	0.27	-0.01
5.333	0.053	5.1	25.0	24.9	2.2	0.28	0.18	-0.00
4.666	0.053	5.8	27.7	27.6	2.8	0.45	0.03	0.02
4.000	0.053	7.5	31.7	31.4	4.1	0.71	-0.07	0.08
3.333	0.053	9.8	37.4	36.8	6.4	0.97	-0.06	0.16
2.666	0.053	13.7	44.8	43.5	10.6	1.12	0.14	0.21
2.000	0.053	17.7	52.3	49.8	15.9	1.21	0.38	0.25
1.333	0.053	23.4	58.4	53.6	23.2	1.32	0.59	0.37
0.666	0.053	34.8	59.5	48.9	34.0	1.29	0.98	0.62
0.000	0.053	63.5	50.8	22.6	45.5	0.68	1.60	0.62

Note: β is in degrees; columns 4 - 9 are expressed as percentages

VERTICAL TRAVERSE JET AT 90 DEGREES

r/d	z/d	β	$\|\bar{V}\|/u_o$	$\bar{u}_r/u_o$	$\bar{v}_\theta/u_o$	$\bar{u}_r^2/u_o^2$	$\bar{v}_\theta^2/u_o^2$	$\overline{u_r v_\theta}/u_o^2$
1.333	0.013	35.6	49.5	40.2	28.8	1.89	1.38	0.68
1.333	0.026	36.0	53.3	43.1	31.4	1.81	1.33	0.69
1.333	0.040	36.8	54.1	43.3	32.4	1.64	1.25	0.63
1.333	0.053	37.4	54.2	43.0	32.9	1.48	1.15	0.57
1.333	0.066	38.3	53.7	42.1	33.3	1.33	1.10	0.50
1.333	0.079	39.2	52.9	41.0	33.5	1.23	1.04	0.44
1.333	0.093	39.3	52.0	40.2	33.0	1.13	1.00	0.39
1.333	0.106	40.3	50.9	38.8	33.0	1.06	0.96	0.34
1.333	0.119	41.5	49.8	37.2	33.0	1.01	0.94	0.32
1.333	0.133	43.0	48.5	35.4	33.1	0.96	0.92	0.28
1.333	0.186	45.8	43.1	30.0	30.9	0.86	0.85	0.27
1.333	0.239	48.1	38.6	25.7	28.7	0.79	0.84	0.30
1.333	0.293	50.7	34.0	21.5	26.3	0.71	0.81	0.33
1.333	0.346	54.1	30.4	17.8	24.7	0.61	0.80	0.34
1.333	0.399	56.5	27.0	14.9	22.6	0.53	0.77	0.31
1.333	0.453	59.9	24.4	12.2	21.1	0.44	0.75	0.30
1.333	0.519	63.3	20.8	9.3	18.6	0.38	0.70	0.26
1.333	0.586	68.8	18.2	6.5	16.9	0.31	0.65	0.21

Note: β is in degrees; columns 4 - 9 are expressed as percentages

VERTICAL TRAVERSE JET AT 90 DEGREES

r/d	z/d	β	$\lvert\bar{V}\rvert/u_o$	$\bar{u}_r/u_o$	$\bar{v}_\theta/u_o$	$\bar{u}_r^2/u_o^2$	$\bar{v}_\theta^2/u_o^2$	$\overline{u_r v_\theta}/u_o^2$
3.000	0.013	27.1	23.6	21.0	10.8	0.76	0.30	0.22
3.000	0.026	26.7	27.3	24.4	12.3	0.88	0.37	0.27
3.000	0.040	28.8	29.3	25.7	14.1	0.88	0.39	0.29
3.000	0.053	30.7	30.1	25.9	15.4	0.85	0.42	0.31
3.000	0.066	32.7	30.3	25.5	16.4	0.80	0.44	0.33
3.000	0.080	34.4	30.3	25.0	17.1	0.75	0.46	0.35
3.000	0.093	36.7	30.4	24.4	18.2	0.71	0.51	0.35
3.000	0.106	38.7	30.1	23.4	18.8	0.68	0.54	0.35
3.000	0.120	40.8	29.7	22.4	19.4	0.64	0.58	0.35
3.000	0.133	42.3	29.3	21.6	19.7	0.61	0.61	0.35
2.999	0.203	46.2	25.5	17.6	18.4	0.53	0.66	0.33
2.999	0.269	50.1	21.1	13.5	16.2	0.43	0.66	0.28
2.999	0.336	56.3	17.1	9.5	14.2	0.33	0.61	0.17
2.999	0.403	61.6	13.5	6.4	11.9	0.25	0.50	0.08

Note: β is in degrees; columns 4 - 9 are expressed as percentages

VERTICAL TRAVERSE JET AT 0 DEGREES

r/d	z/d	β	$\|\overline{V}\|/u_o$	$\overline{u}_r/u_o$	$\overline{v}_\theta/u_o$	$\overline{u}_r^2/u_o^2$	$\overline{v}_\theta^2/u_o^2$	$\overline{u_r v_\theta}/u_o^2$
1.333	0.013	0.0	64.6	64.6	0.0	2.36	0.77	0.01
1.333	0.026	0.0	68.0	68.0	0.0	2.48	0.65	0.00
1.333	0.040	0.0	71.4	71.4	0.0	2.39	0.53	0.01
1.333	0.053	0.0	72.2	72.2	0.0	2.17	0.42	0.01
1.333	0.080	0.0	72.0	72.0	0.0	1.87	0.41	0.01
1.333	0.106	0.0	70.7	70.7	0.0	1.49	0.39	0.01
1.333	0.133	0.0	68.8	68.8	0.0	1.24	0.41	0.01
1.333	0.160	0.0	66.3	66.3	0.0	1.12	0.46	0.01
1.333	0.186	0.0	63.7	63.7	0.0	1.07	0.50	0.01
1.333	0.213	0.0	60.9	60.9	0.0	1.05	0.55	0.00
1.333	0.240	0.0	58.1	58.1	0.0	1.07	0.58	0.00
1.333	0.266	0.0	55.2	55.2	0.0	1.09	0.61	0.01
1.333	0.293	0.0	52.7	52.7	0.0	1.10	0.66	0.01
1.333	0.319	0.0	50.0	50.0	0.0	1.14	0.64	0.01
1.333	0.453	0.0	37.8	37.8	0.0	1.23	0.52	0.01
1.333	0.586	0.0	28.0	28.0	0.0	1.10	0.35	0.01
1.333	0.719	0.0	20.5	20.5	0.0	0.85	0.25	0.02
1.333	0.853	0.0	14.4	14.4	0.0	0.60	0.15	0.01
1.333	0.986	0.0	10.2	10.2	0.0	0.35	0.10	0.00
1.333	1.120	0.0	7.0	7.0	0.0	0.17	0.07	0.00
1.333	1.253	0.0	5.3	5.3	0.0	0.07	0.03	0.00
1.333	1.386	0.0	4.2	4.2	0.0	0.02	0.01	0.00

Note: β is in degrees; columns 4 - 9 are expressed as percentages

VERTICAL TRAVERSE JET AT 45 DEGREES

r/d	z/d	β	$\|\overline{V}\|/u_o$	$\overline{u}_r/u_o$	$\overline{v}_\theta/u_o$	$\overline{u_r^2}/u_o^2$	$\overline{v_\theta^2}/u_o^2$	$\overline{u_r v_\theta}/u_o^2$
1.333	0.013	17.0	68.8	65.8	20.1	2.59	0.77	0.53
1.333	0.026	17.5	70.4	67.1	21.2	2.41	0.65	0.53
1.333	0.040	17.7	70.7	67.3	21.5	2.14	0.62	0.49
1.333	0.053	17.7	70.3	67.0	21.4	1.90	0.61	0.42
1.333	0.066	18.2	69.4	65.9	21.7	1.73	0.59	0.38
1.333	0.079	18.7	68.2	64.6	21.9	1.57	0.60	0.34
1.333	0.093	18.3	67.1	63.6	21.4	1.46	0.61	0.31
1.333	0.106	19.1	65.5	61.9	21.4	1.36	0.62	0.27
1.333	0.119	19.6	64.1	60.4	21.5	1.29	0.65	0.23
1.333	0.133	20.4	62.7	58.8	21.9	1.24	0.67	0.24
1.333	0.186	19.8	57.6	54.5	18.6	1.13	0.69	0.15
1.333	0.239	20.1	51.5	48.4	17.7	1.13	0.69	0.15
1.333	0.293	22.0	46.6	43.2	17.4	1.13	0.68	0.16
1.333	0.346	22.1	41.1	38.0	15.5	1.14	0.62	0.21
1.333	0.399	24.3	37.1	33.8	15.3	1.10	0.56	0.24
1.333	0.453	25.6	32.8	29.6	14.2	1.03	0.48	0.29
1.333	0.506	24.5	29.6	26.9	12.3	1.05	0.33	0.39
1.333	0.559	26.8	26.0	23.2	11.8	0.87	0.37	0.30
1.333	0.613	23.3	22.7	20.8	9.0	0.78	0.31	0.26
1.333	0.666	27.2	19.7	17.5	9.0	0.68	0.30	0.24
1.333	0.719	28.0	17.7	15.6	8.3	0.60	0.26	0.24
1.333	0.773	27.0	15.2	13.5	6.9	0.53	0.23	0.18
1.333	0.826	25.3	13.7	12.4	5.9	0.46	0.18	0.17
1.333	0.879	24.4	12.4	11.3	5.1	0.38	0.15	0.15
1.333	0.933	25.3	10.7	9.6	4.5	0.31	0.10	0.13
1.333	0.986	24.7	8.6	7.8	3.6	0.23	0.13	0.05
1.333	1.039	24.0	7.9	7.2	3.2	0.19	0.11	0.05

Note: β is in degrees; columns 4 - 9 are expressed as percentages

VERTICAL TRAVERSE JET AT 45 DEGREES

r/d	s/d	β	$\lvert\bar{V}\rvert/u_o$	$\bar{u}_r/u_o$	$\bar{v}_\theta/u_o$	$\bar{u}_r^2/u_o^2$	$\bar{v}_\theta^2/u_o^2$	$\overline{u_r v_\theta}/u_o^2$
3.000	0.013	8.9	50.2	49.6	7.7	1.94	0.69	0.00
3.000	0.026	9.5	52.8	52.0	8.7	1.82	0.63	0.05
3.000	0.039	8.9	53.4	52.7	8.3	1.77	0.62	0.05
3.000	0.053	8.7	53.8	53.2	8.2	1.68	0.64	0.05
3.000	0.066	8.8	53.6	52.9	8.2	1.61	0.68	0.06
3.000	0.079	8.4	52.9	52.3	7.7	1.59	0.64	0.09
3.000	0.093	8.6	52.1	51.5	7.8	1.54	0.66	0.10
3.000	0.106	8.9	51.0	50.4	7.9	1.52	0.69	0.12
3.000	0.119	8.9	50.1	49.5	7.7	1.51	0.69	0.13
3.000	0.133	9.0	49.0	48.4	7.6	1.51	0.73	0.13
3.000	0.186	9.4	43.3	42.8	7.1	1.56	0.73	0.18
3.000	0.240	10.3	37.7	37.1	6.7	1.52	0.69	0.21
3.000	0.293	12.1	32.0	31.3	6.7	1.40	0.65	0.23
3.000	0.346	14.0	26.7	25.9	6.4	1.25	0.55	0.25
3.000	0.400	14.2	22.3	21.6	5.4	1.01	0.51	0.23
3.000	0.453	15.8	18.5	17.8	5.0	0.79	0.44	0.21
3.000	0.506	15.1	15.3	14.8	4.0	0.60	0.37	0.16
3.000	0.560	16.5	12.8	12.2	3.6	0.42	0.31	0.11
3.000	0.613	15.3	10.8	10.4	2.8	0.32	0.25	0.07
3.000	0.666	14.9	9.2	8.9	2.3	0.23	0.18	0.04
3.000	0.720	14.4	8.0	7.7	1.8	0.16	0.14	0.02
3.000	0.773	14.9	7.1	6.9	1.8	0.11	0.10	0.00
3.000	0.826	12.1	6.4	6.3	1.3	0.07	0.07	0.00
3.000	0.879	12.1	5.8	5.6	1.4	0.05	0.05	0.00
3.000	0.933	11.0	5.4	5.3	1.0	0.03	0.03	0.00
3.000	0.986	10.3	5.2	5.1	0.9	0.02	0.02	0.00
3.000	1.040	5.5	4.9	4.8	0.4	0.01	0.01	0.00

Note: β is in degrees; columns 4 - 9 are expressed as percentages

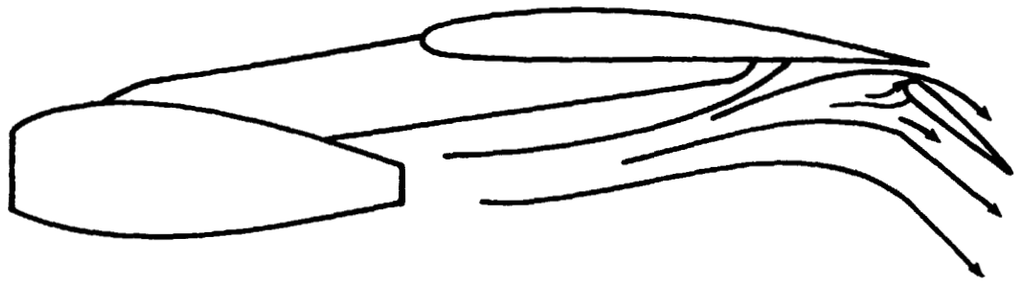

Figure 1. The externally blown flap configuration for STOL aircraft.

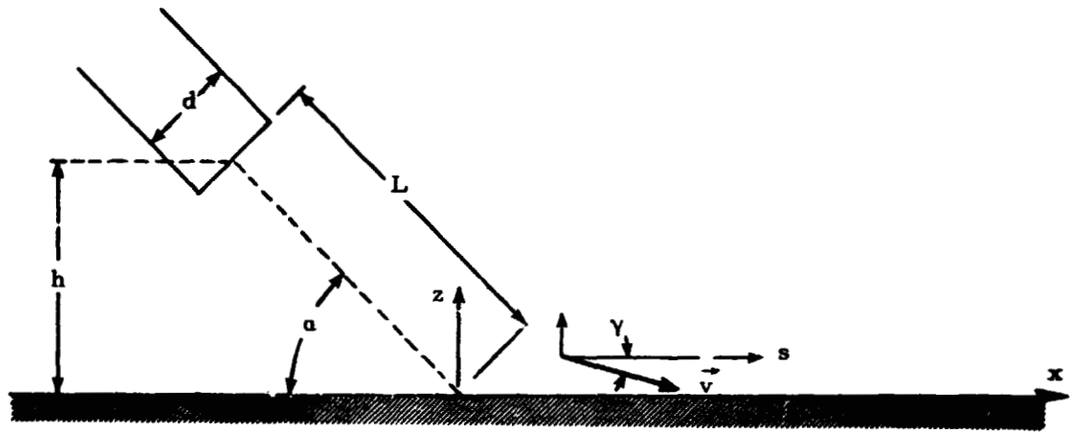

a. Side View

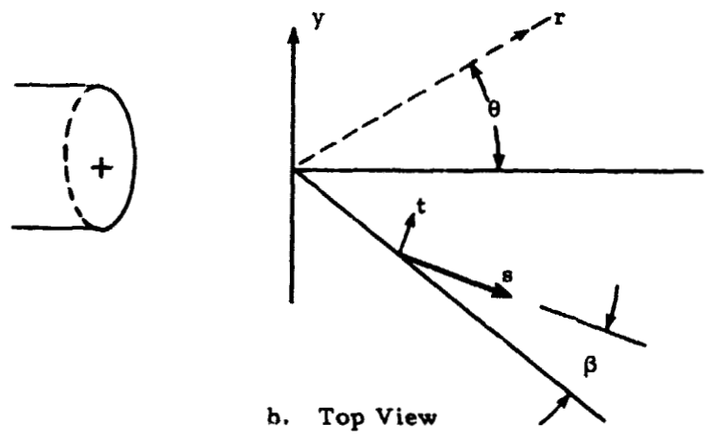

b. Top View

Figure 2. Nomenclature for the oblique jet impingement flow.

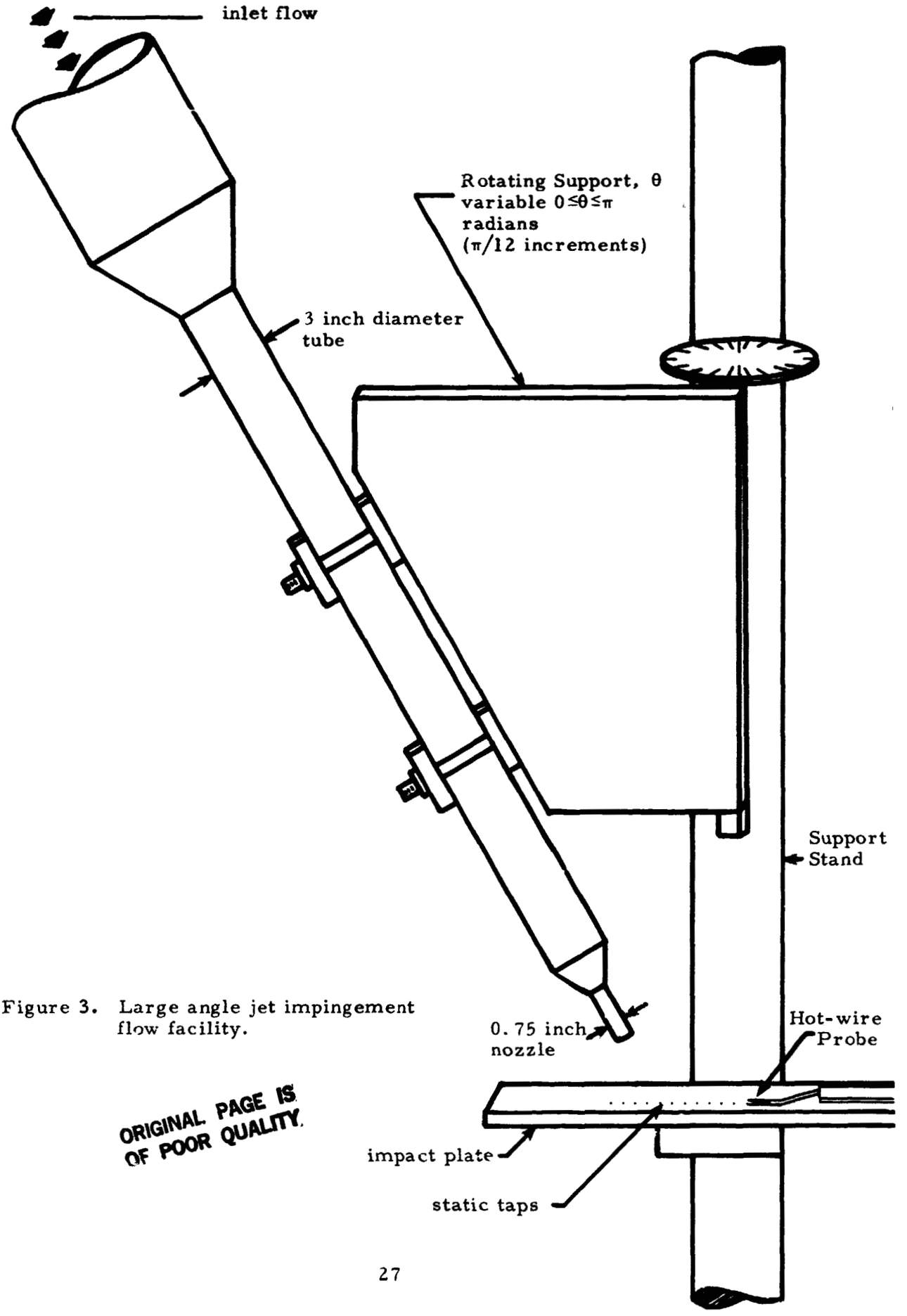

Figure 3. Large angle jet impingement flow facility.

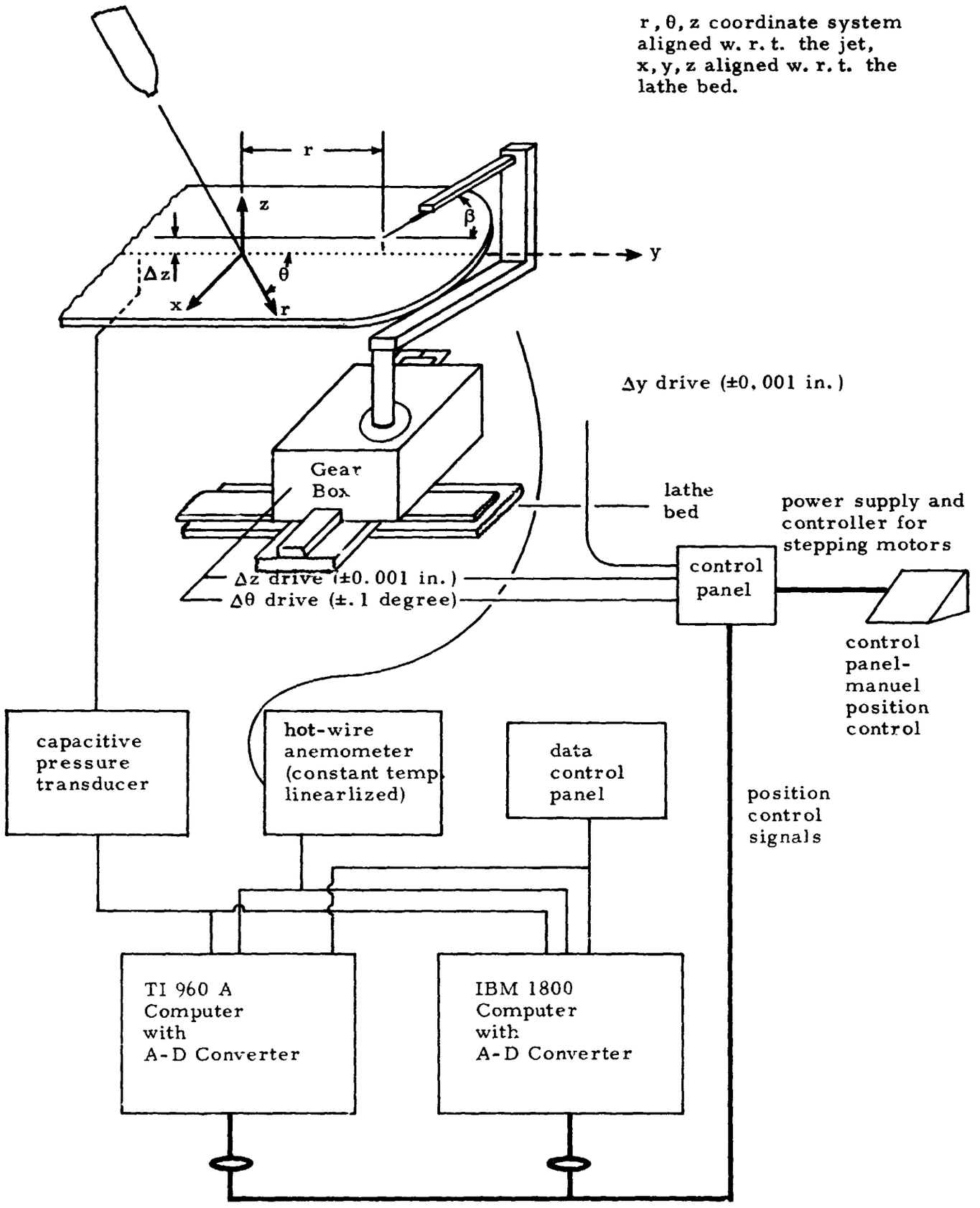

Figure 4. Schematic of data acquisition facility.

NOTE:

d = 0.75 inch

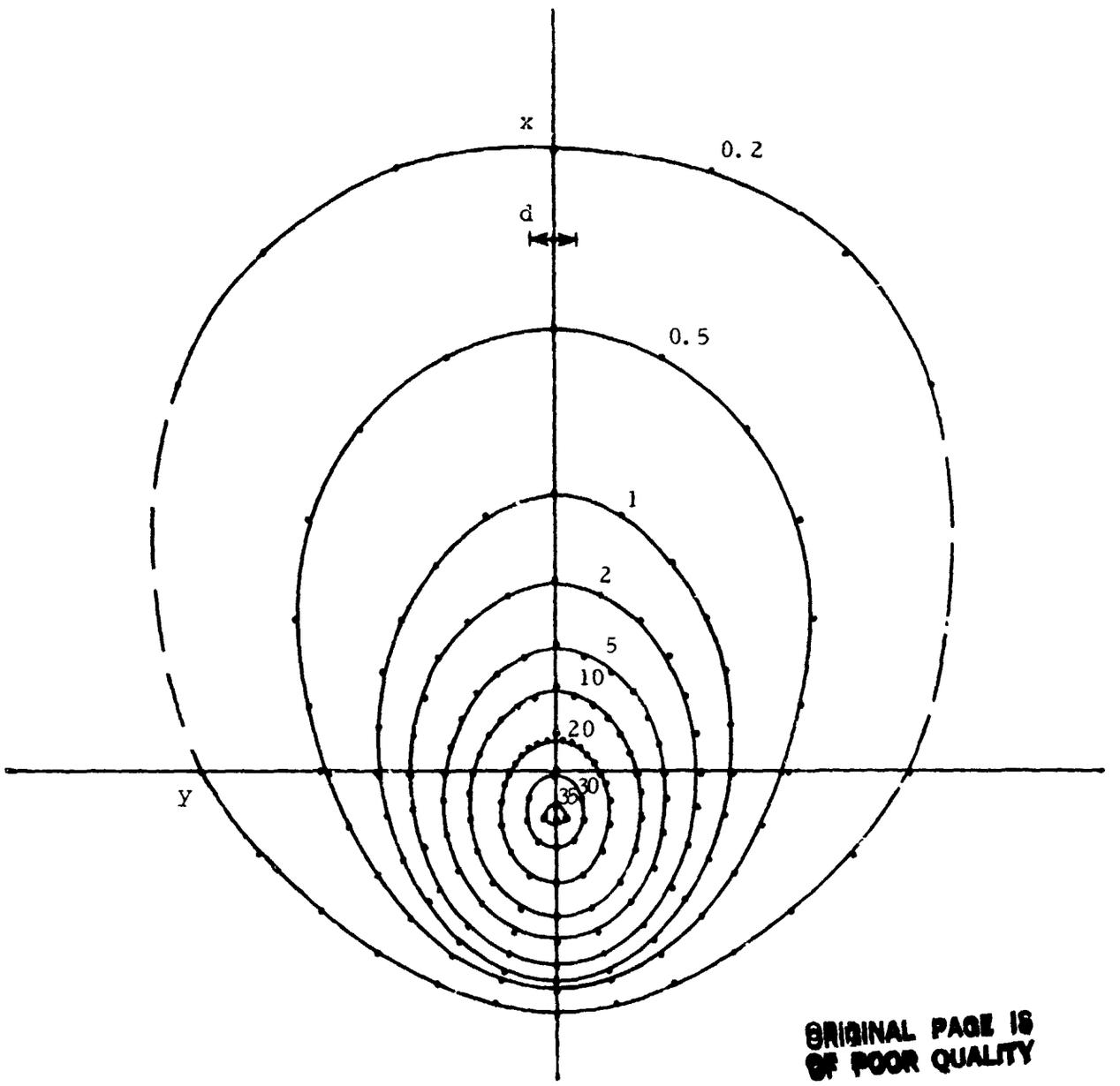

Figure 5. Surface pressure isobar contours. $\alpha = 45$ degrees, $L/d = 7$, jet Reynolds number $= 4.8 \times 10^4$.

Contours represent level curves of $100 \dfrac{(p - p_{atm})}{\rho u_o^2 \lambda \sin \alpha}$

$\lambda = \int_{A_{jet}} \rho u^2 \, dA / \rho u_p^2 A_{jet}$, $\lambda = 0.809$ taken from [5].

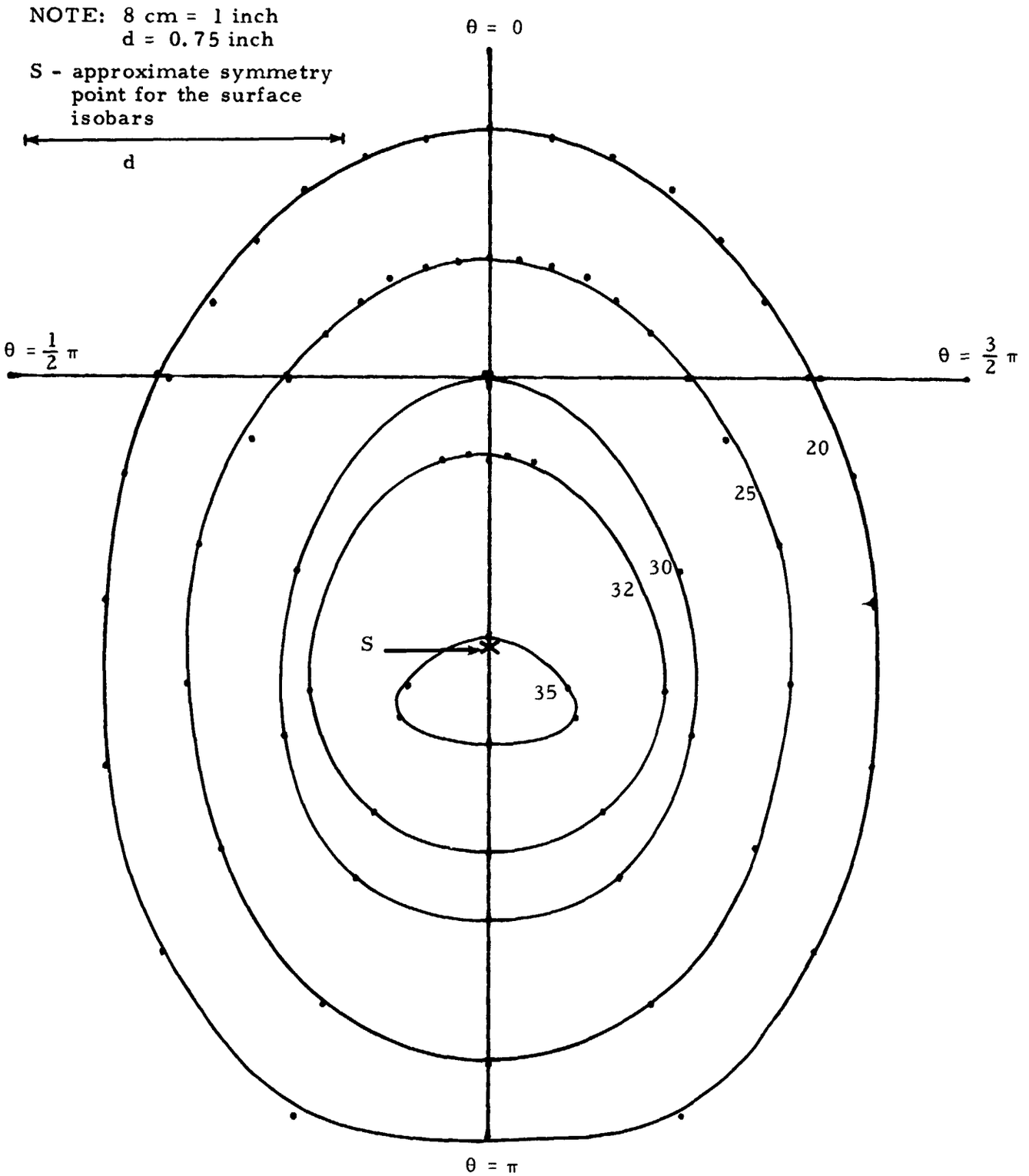

Figure 6. Expanded scale to show detail of the maximum pressure region.

Figure 7. Velocity magnitude traverses in the $\theta = 0$, $\theta = \pi$ plane.

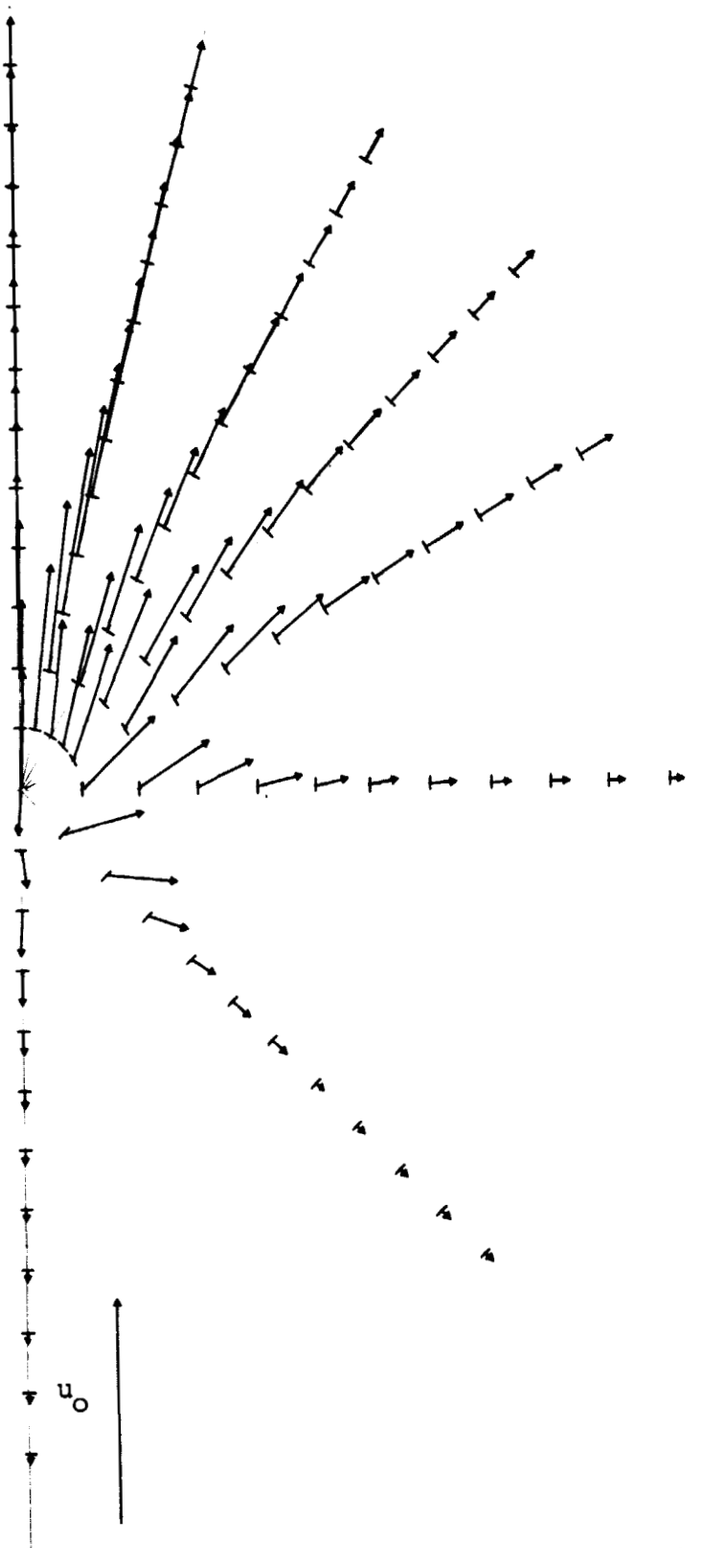

Figure 8. Composite view of the time mean velocity field in the plane z/d = 0.053.

Length scale of plot: data points acquired for each 2d/3 along the radial lines shown.

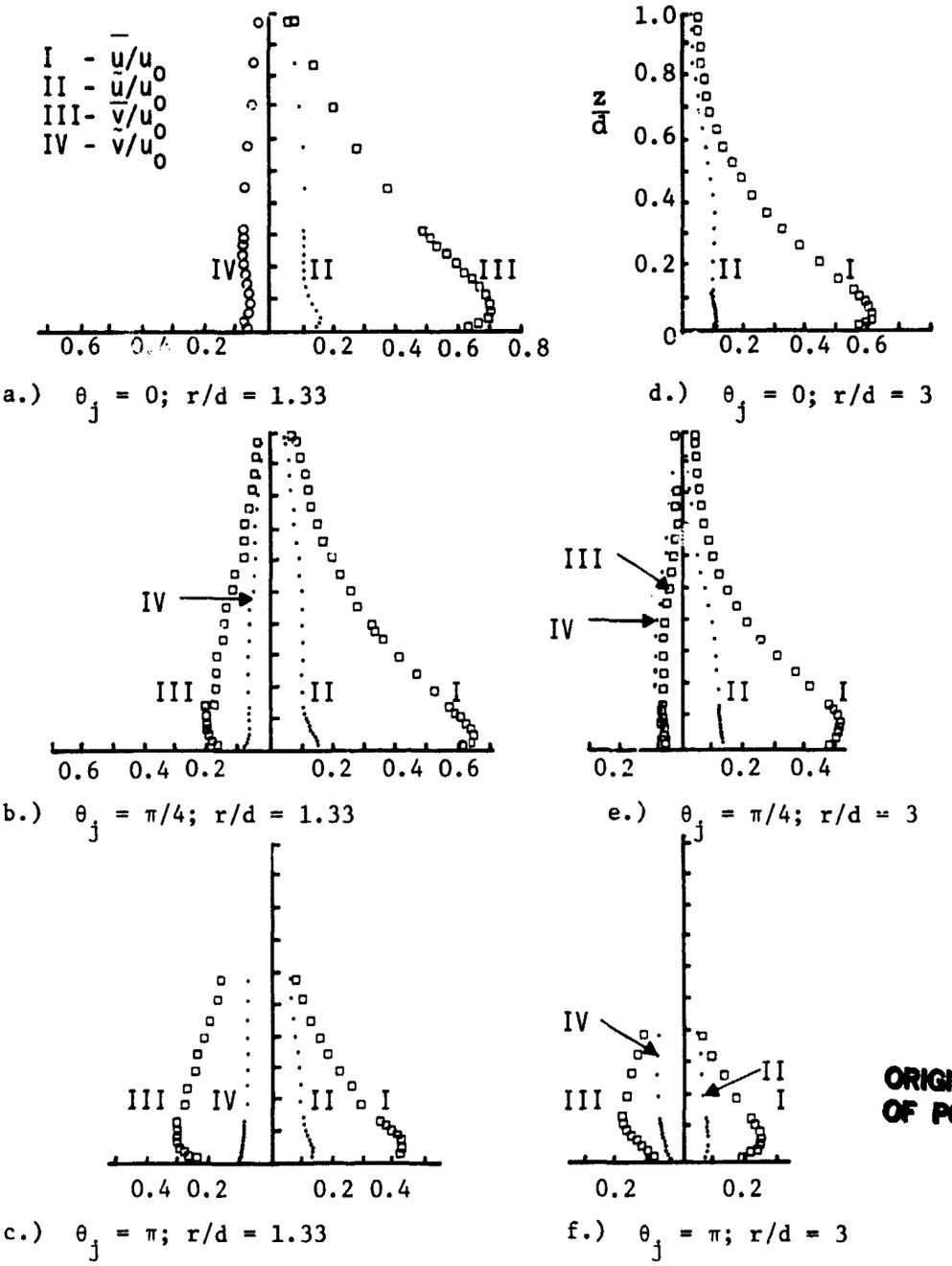

Figure 9. Vertical traverses of the velocity field

Note: The z/d axis of Figure 9d is common to (a-f).

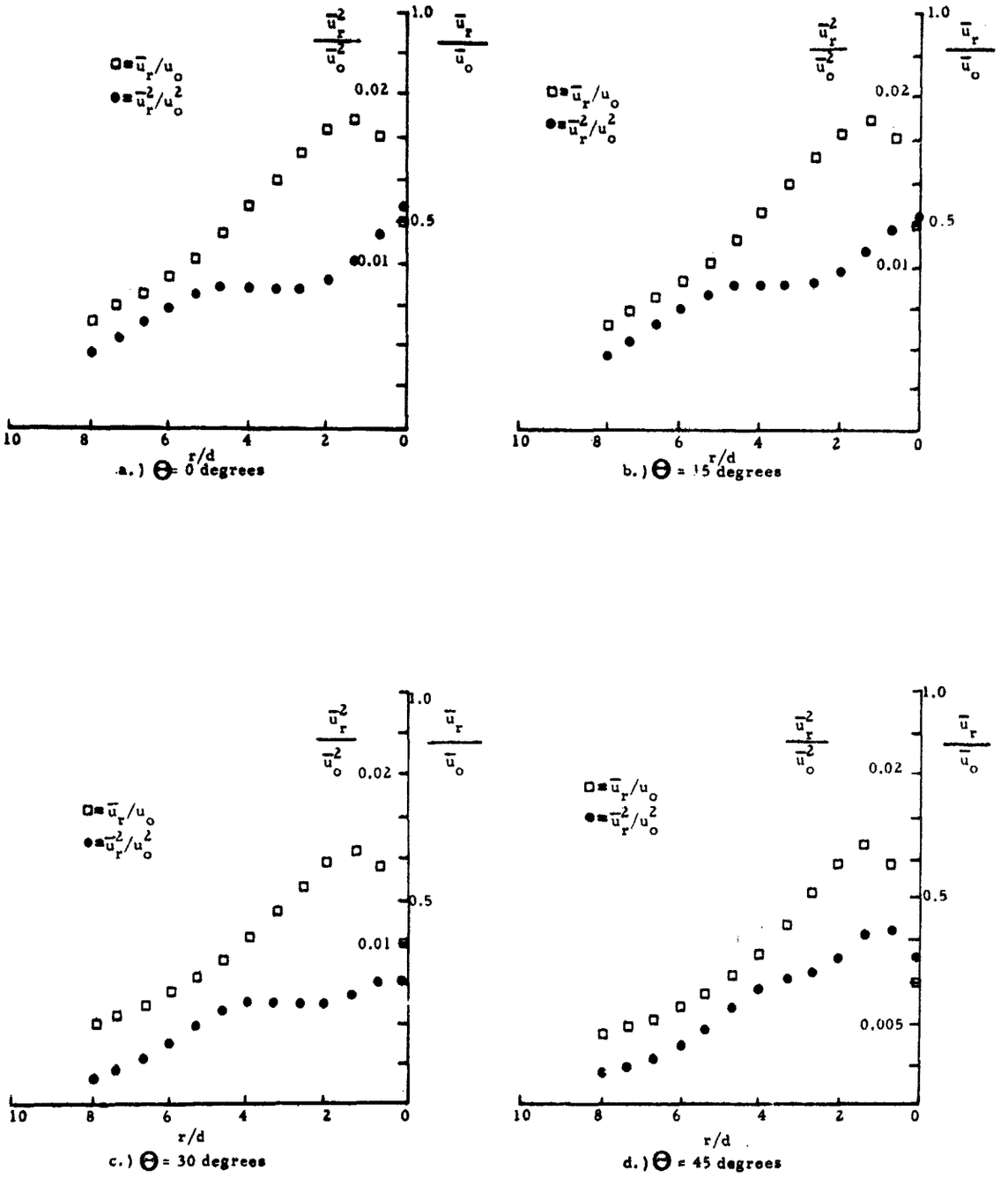

Figure 10. Radial traverses of the radial velocity and the normal Reynolds stress. (Presentation is to allow the magnitude of $\overline{u}_r^2$ $\partial\overline{u}_r/\partial r$.)

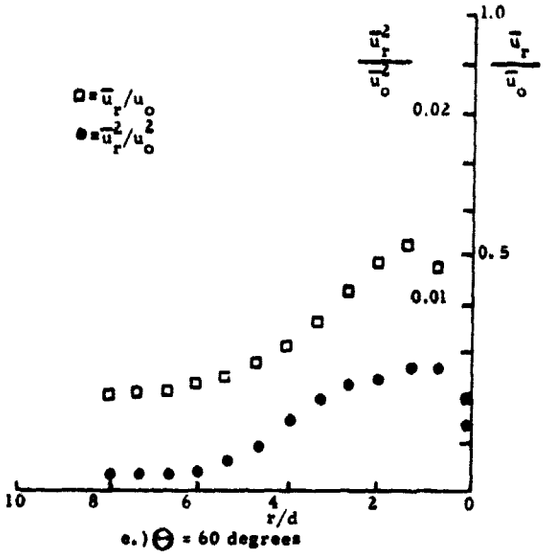

e.) Θ = 60 degrees

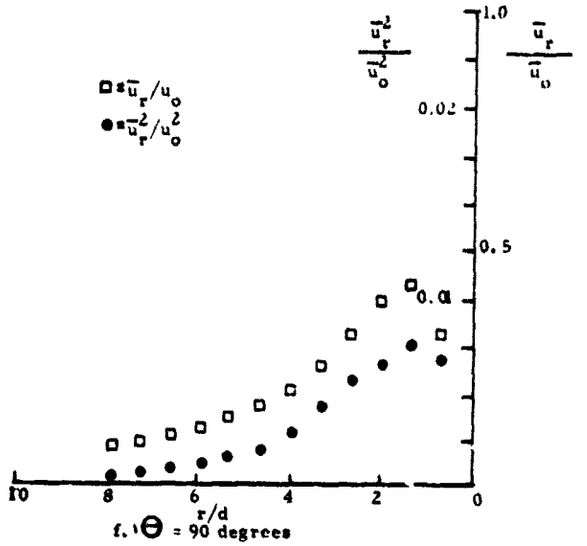

f.) Θ = 90 degrees

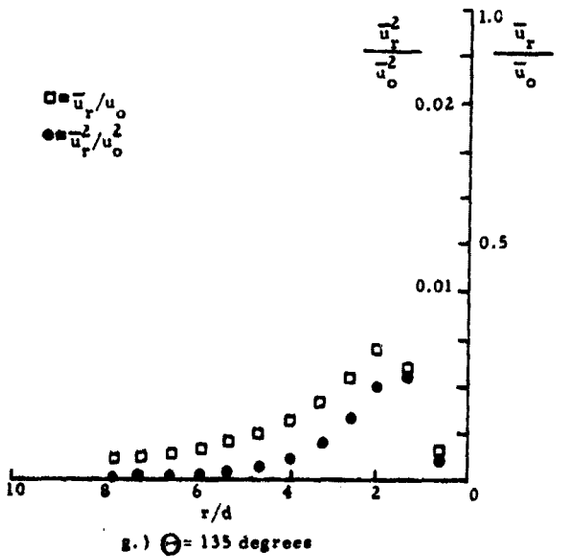

g.) Θ = 135 degrees

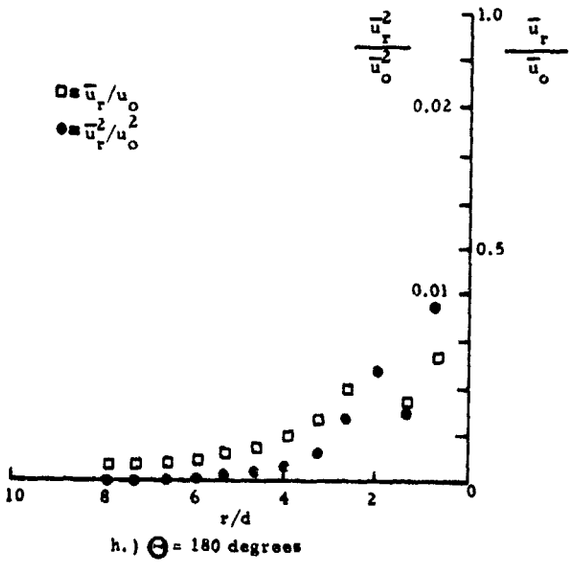

h.) Θ = 180 degrees

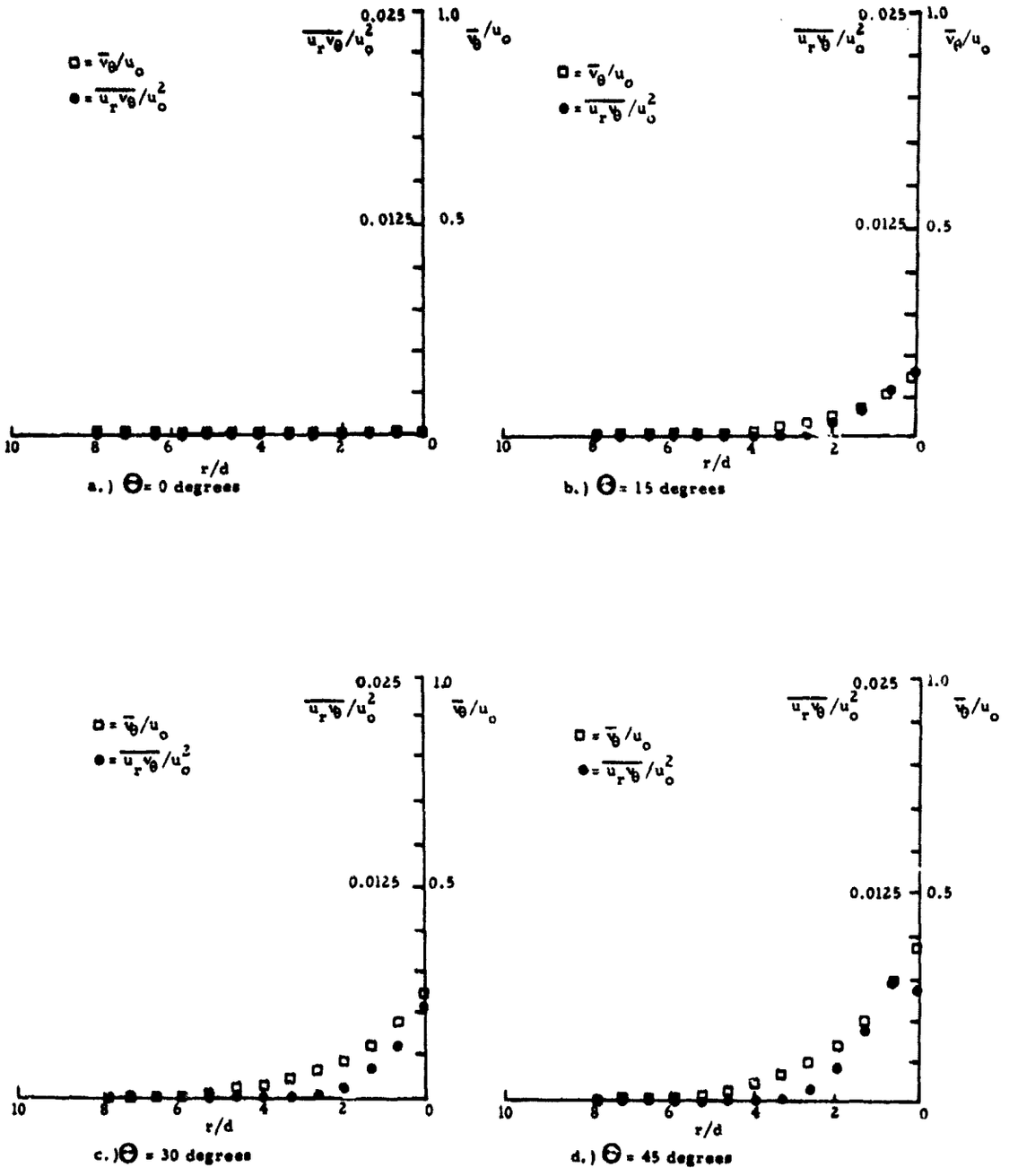

Figure 11. Radial traverses of the azimuthal velocity and the Reynolds shear stress. (Presentation is to allow the magnitude of $\overline{u_r v_\theta}$ $\partial v_\theta/\partial r$ to be inferred.)

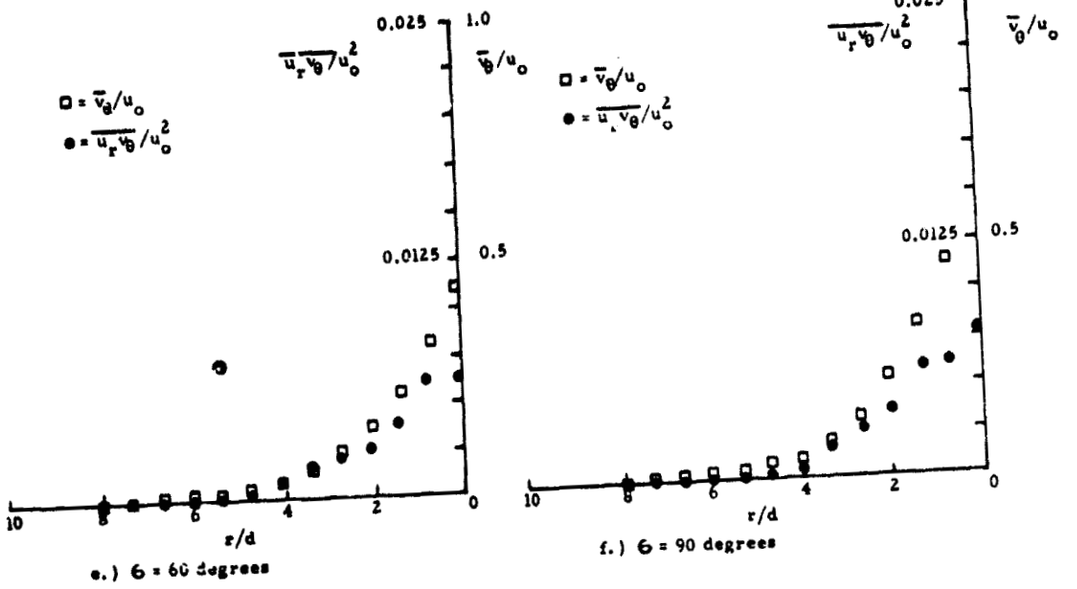

e.) θ = 60 degrees

f.) θ = 90 degrees

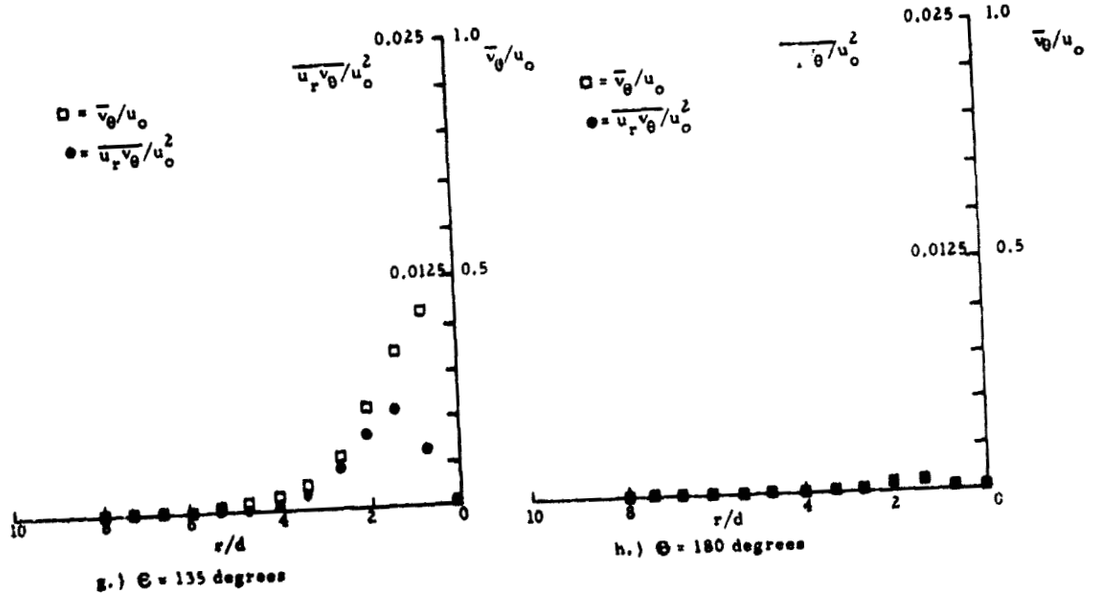

g.) θ = 135 degrees

h.) θ = 180 degrees

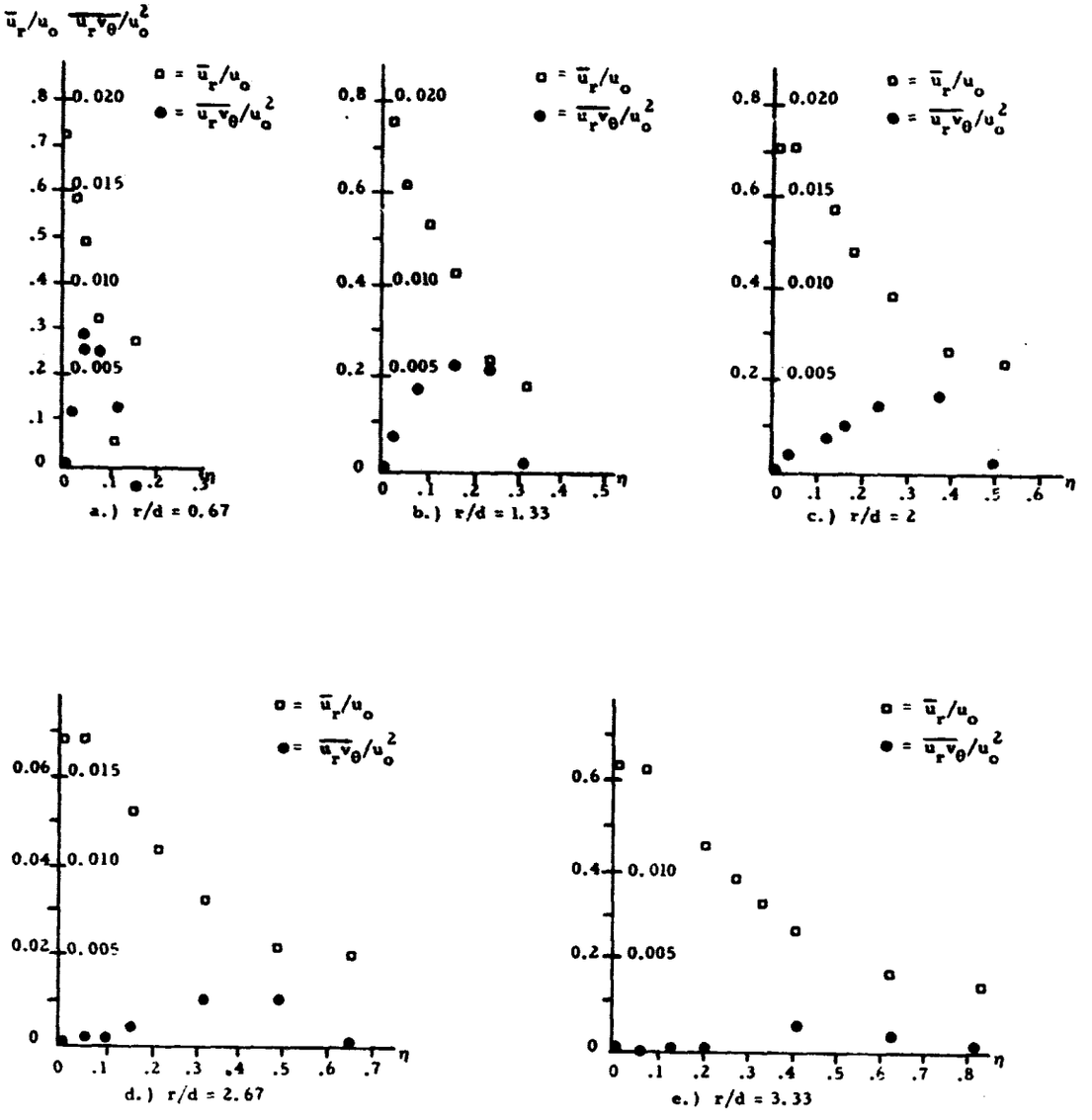

NOTE: The coordinate η ($\eta = [r\theta/d]\,1[r\theta/d]_{reference}$) is arbitrarily defined such that $r\theta/d_{reference} = 4\pi$

Figure 12. Azimuthal distributions of the radial velocity and Reynolds shear stress. (Presentation is to allow the magnitude of $\overline{u_r v_\theta}\ \partial\bar{u}_r/\partial r\theta$ to be inferred)

$\bar{u}_r/u_o$ $\overline{u_r v_\theta}/u_o^2$

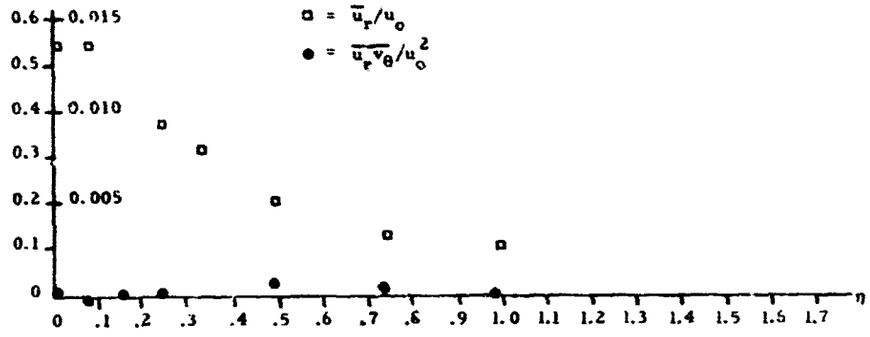

f.) r/d = 4.0

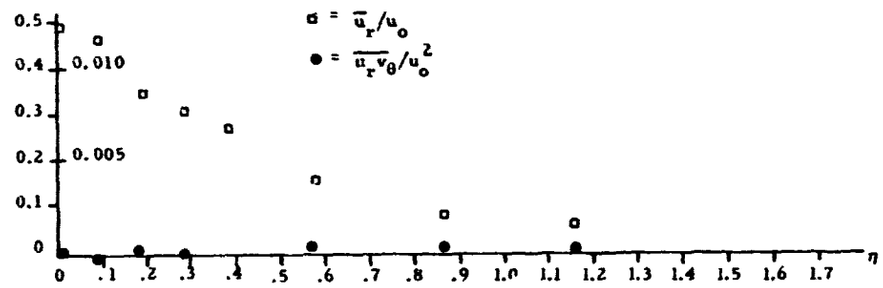

g.) r/d = 4.67

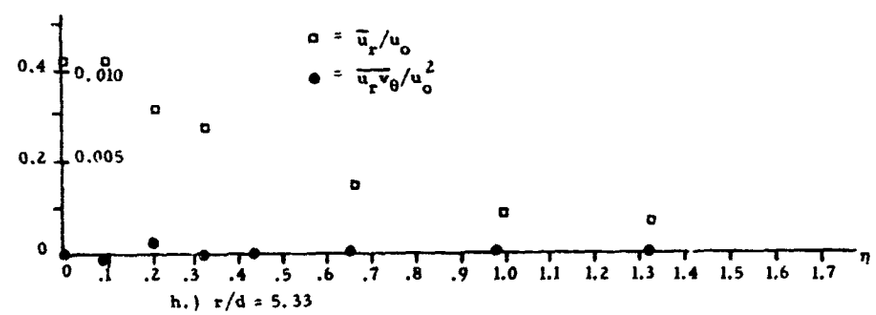

h.) r/d = 5.33

$\bar{u}_r/u_o$ $\overline{u_r v_\theta}/u_o^2$

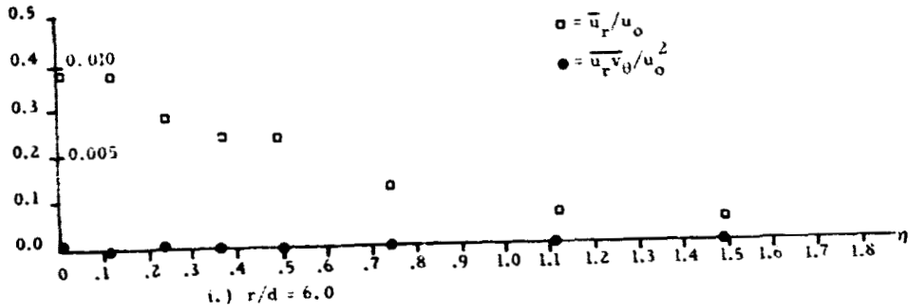

i.) r/d = 6.0

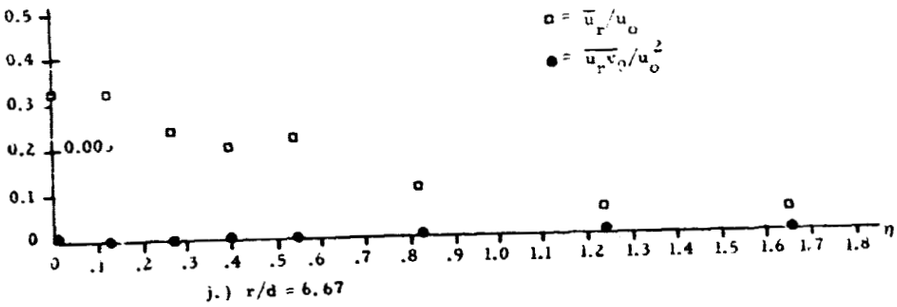

j.) r/d = 6.67

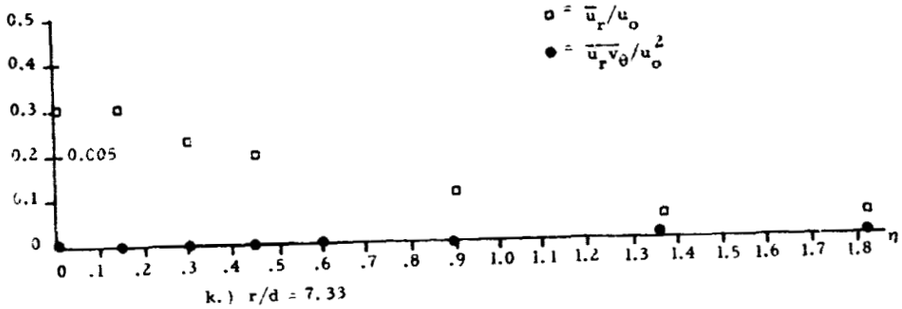

k.) r/d = 7.33

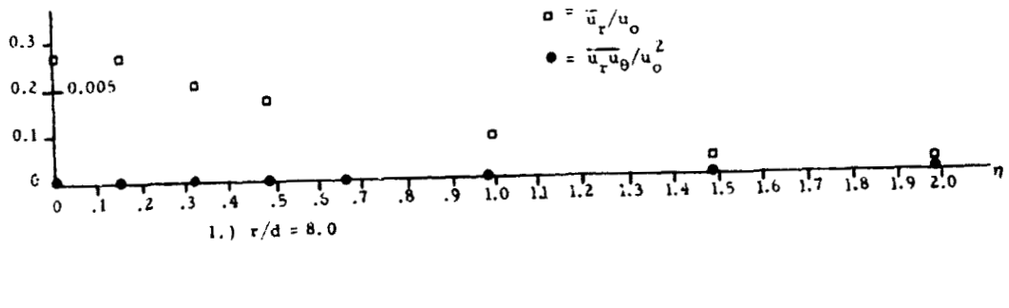

l.) r/d = 8.0

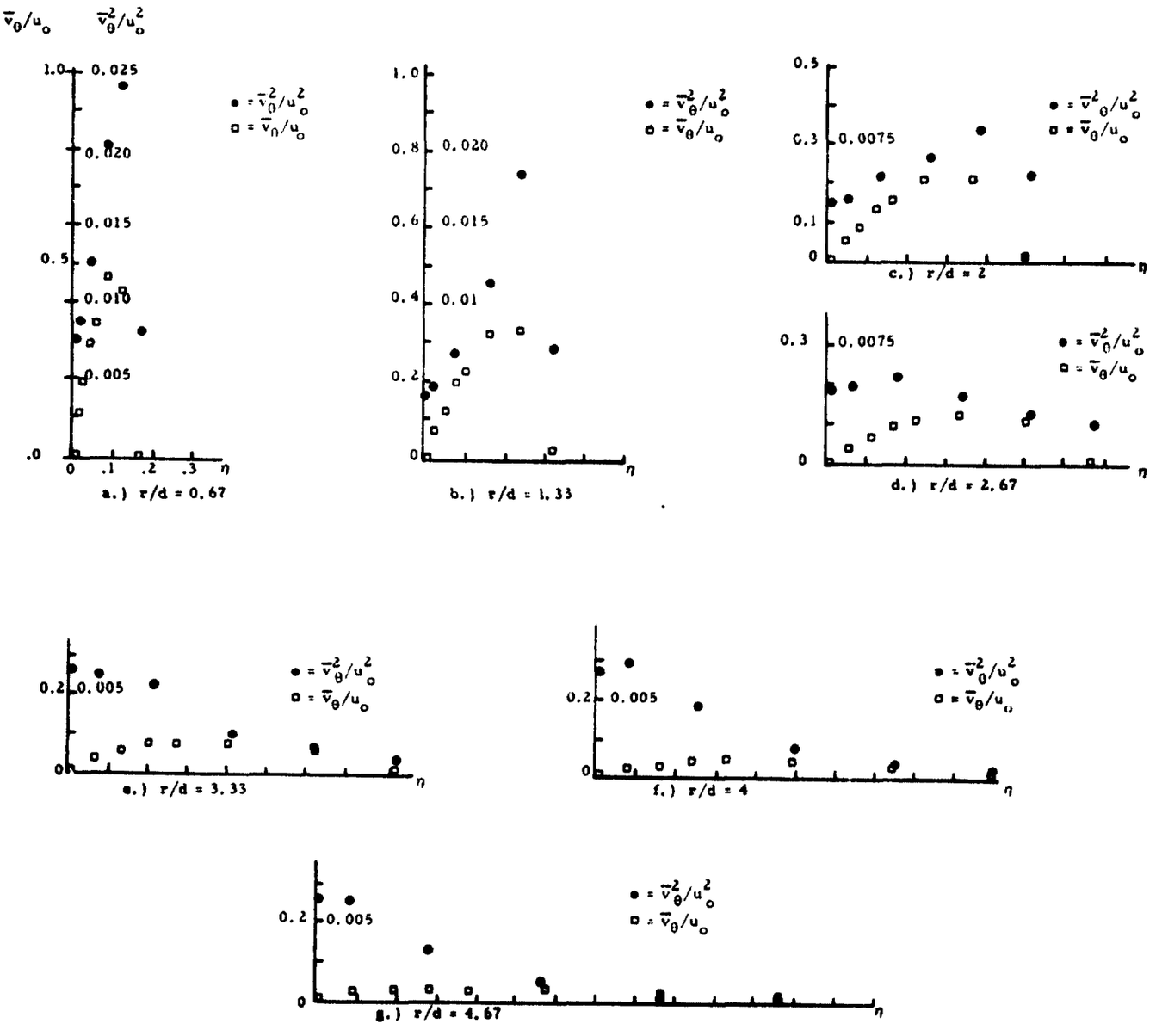

Figure 13. Azimuthal distributions of the azimuthal velocity and the azimuthal Reynolds stress. (Presentation is to allow the magnitude of $\overline{v_\theta^2}$ $\partial\overline{v}_\theta/\partial\, r\theta$ to be inferred.)

Note: The coordinate η ($\eta \equiv [r\theta/d]/[r\theta/d]_{\text{reference}}$) is arbitrarily defined such that $[r\theta/d]_{\text{reference}} = 4\pi$.

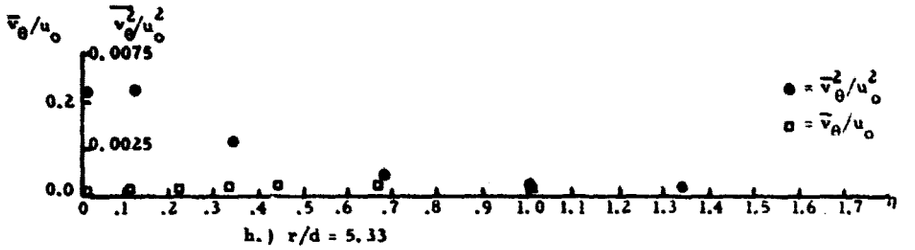

h.) r/d = 5.33

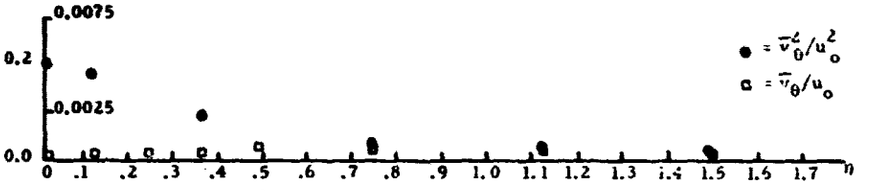

i.) r/d = 6.0

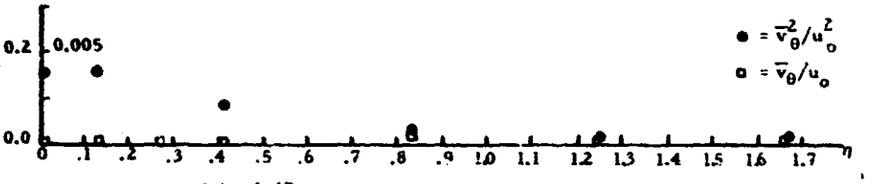

j.) = 6.67

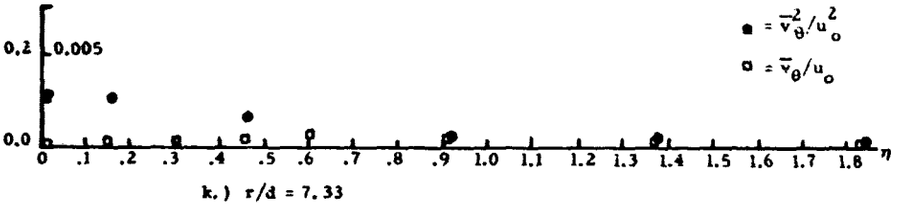

k.) r/d = 7.33

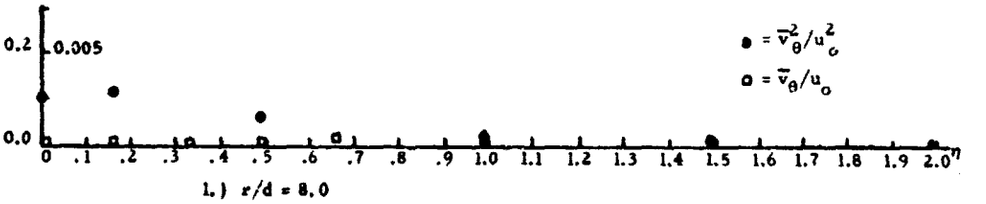

l.) r/d = 8.0

NOTE: The coordinate η ($\eta = [r\theta/d] / [r\theta/d]_{\text{reference}}$) is arbitrarily defined such that $r\theta/d_{\text{reference}} = 4\pi$

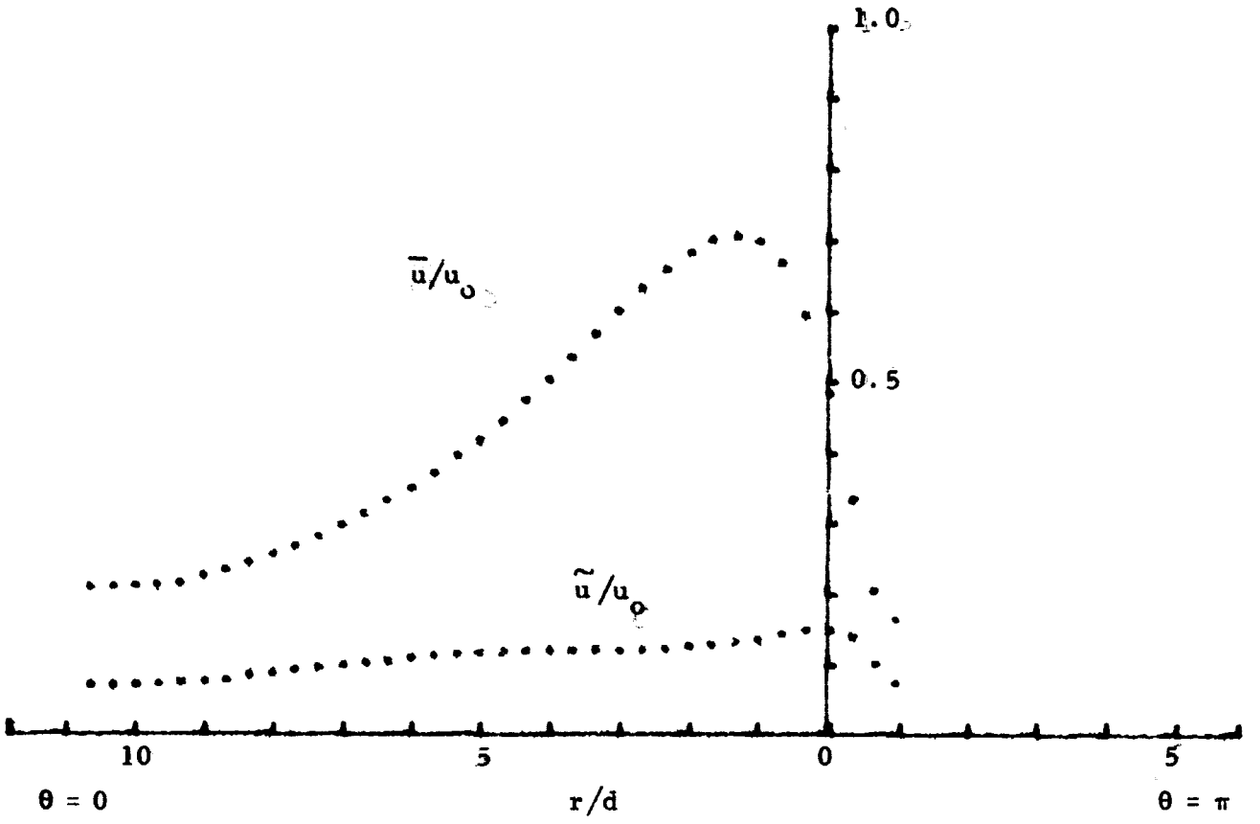

Figure 14. $\bar{u}/u_o$ and $\tilde{u}/u_o$ vs r/d for the θ = 0 plane, z/d = 0.04 (h/d = 7, jet Reynolds number = $u_o d/\nu$ = 4.8×10^4).

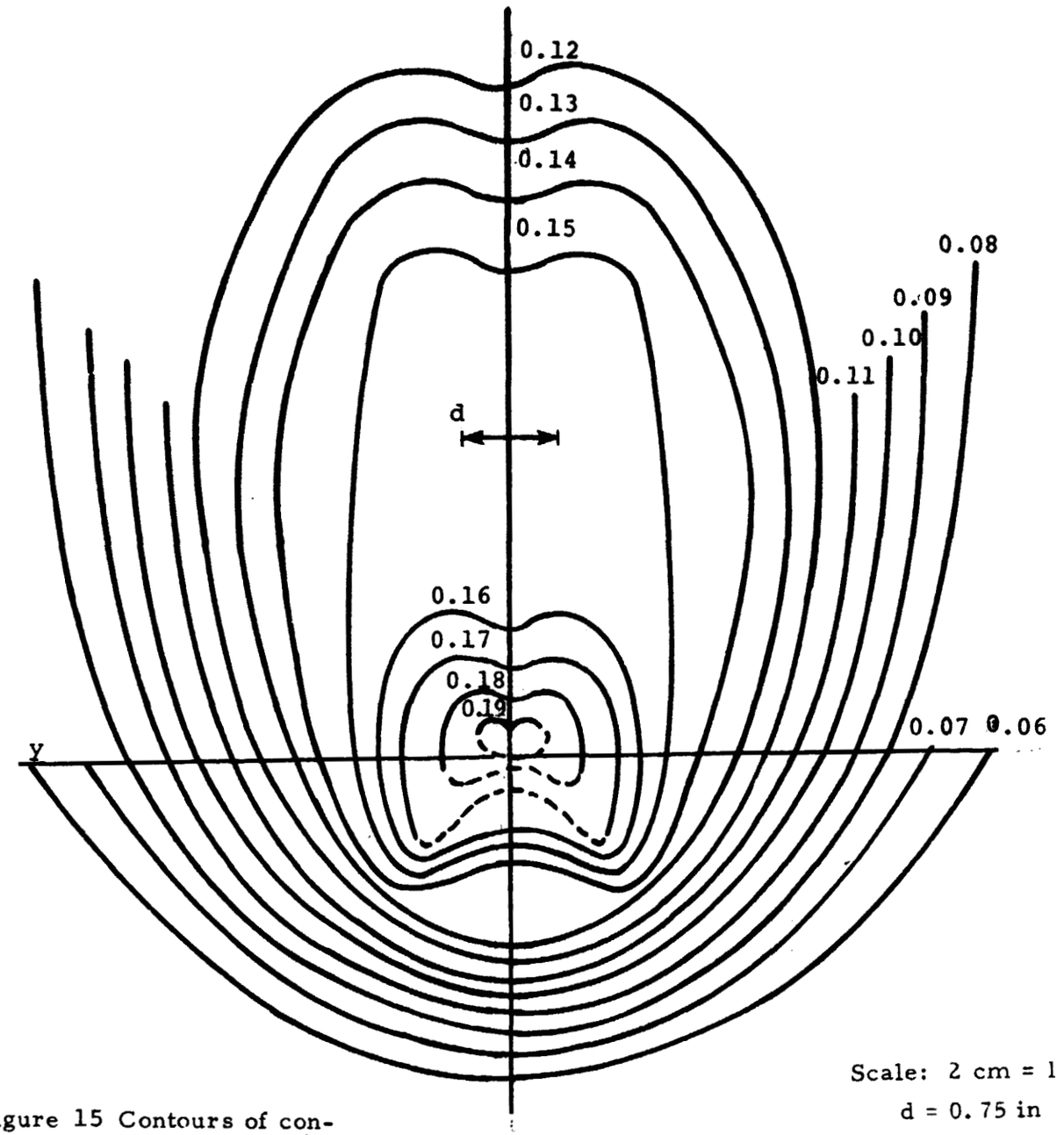

Scale: 2 cm = 1 in
d = 0.75 in

Figure 15 Contours of constant intensity $(\overline{u}_r^2 + \overline{v}_\theta^2)^{1/2} / u_o$ in the plane z/d = 0.053, conditions: L/d = 7, $R_e = 4.8 \times 10^4$, α = 45 degrees.

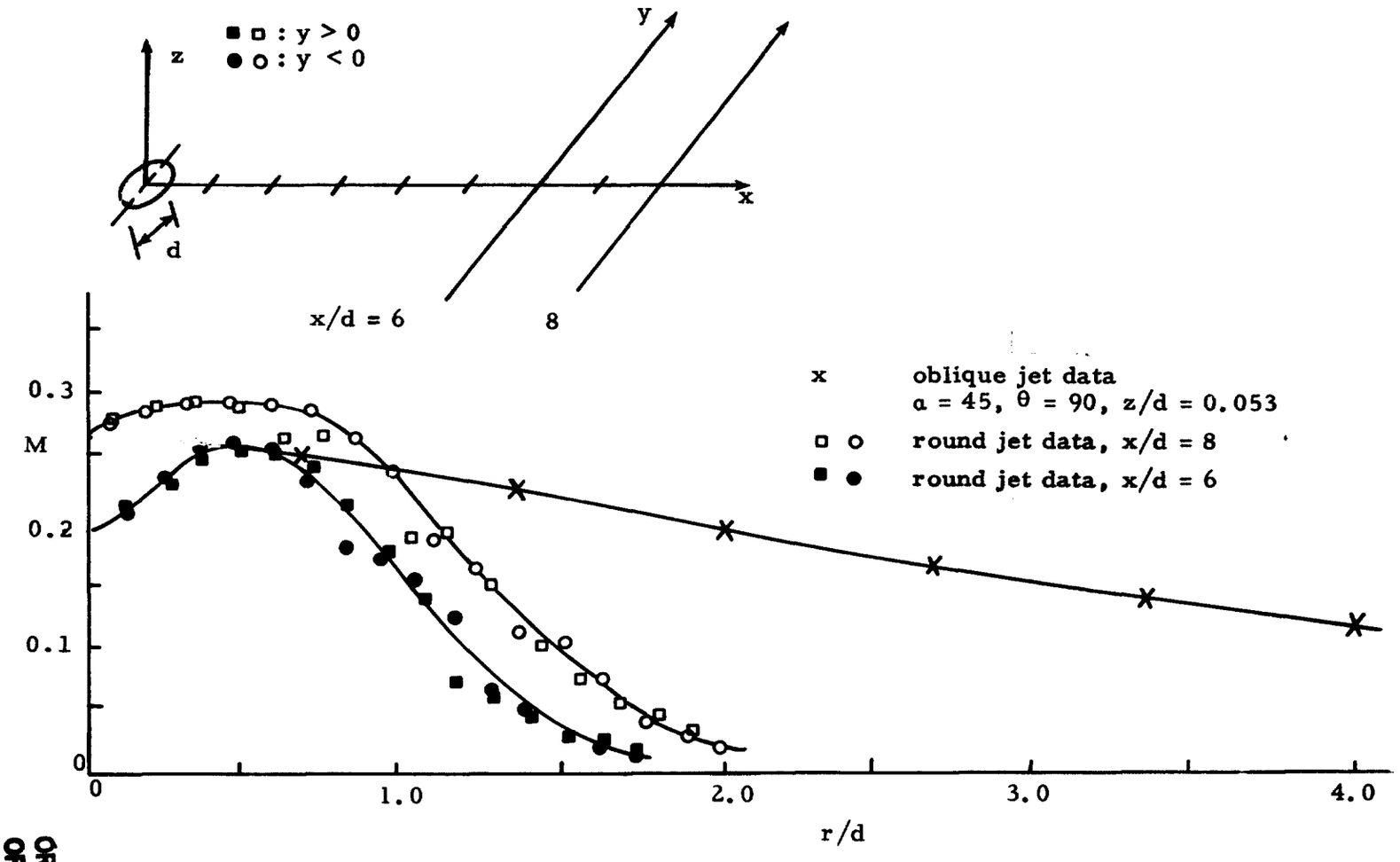

Figure 16. Comparison of turbulence intensity magnitudes from a free and the impinging jet flows. Note $M = (\tilde{u} + \tilde{v})/u_o$ for the axisymmetric jet and $(\tilde{u}_r + \tilde{v}_\theta)/u_o$ for the oblique impingement flow.